TRITA-EPP-90-01

LABORATORY EXPERIMENTS ON THE MAGNETIC FIELD AND NEUTRAL DENSITY LIMITS ON CIV INTERACTION

I. Axnäs and N. Brenning

TRITA-EPP-90-01 .

LABORATORY EXPERIMENTS ON THE MAGNETIC FIELD AND NEUTRAL DENSITY LIMITS ON CIV INTERACTION

I. Axnäs and N. Brenning

March 1990

Department of Plasma Physics
The Royal Institute of Technology
S-100 44, Stockholm, Sweden.

LABORATORY EXPERIMENTS ON THE MAGNETIC FIELD AND NEUTRAL DENSITY LIMITS ON CIV INTERACTION

I. Axnäs and N. Brenning
The Royal Institute of Technology, Department of Plasma Physics,
S-100 44, Stockholm, Sweden.

Abstract

Laboratory experiments are reported which determine the magnetic field and neutral density limits for Critical Ionization Velocity (CIV) interaction in the impact configuration. A combination of microwave interferometry and spectroscopy has been used to measure how the electron energy distribution varies with the neutral density and the magnetic field strength. The efficiency of the CIV process is evaluated in terms of the efficiency factor η of energy transfer to the electrons. This efficiency is studied as function of the ratio V_A/V_0 between the Alfvén velocity and the plasma stream velocity and the ratio ν_i/ω_{gi} between the ionization frequency and the ion gyro frequency. With other parameters kept constant, V_A/V_0 is proportional to the square root of the magnetic field, while ν_i/ω_{gi} is proportional to the neutral density. We have found that these two dimensionless parameters are coupled in such a fashion that a stronger magnetic field can compensate for a lower neutral density. For our strongest magnetic field, corresponding to $V_A/V_0 = 4$, CIV interaction is found to occur for a comparatively low value $\nu_i/\omega_{gi} \approx 0.1$. For $V_A/V_0 = 1$, we found a clear absence of CIV interaction even for ν_i/ω_{gi} approaching unity.

1. Introduction.

The Critical Ionization Velocity (CIV) process applies to situations where a plasma is streaming through a neutral gas. The CIV process uses the kinetic energy in the relative motion for ionization of the neutral gas. In connection with his theory for the formation of the solar system, Alfvén (1942, 1954) proposed that such ionization should occur in cases where the plasma is penetrated by a transverse magnetic field, and where the relative velocity exceeds a critical value V_c. At the velocity V_c the kinetic energy of the neutrals, in the plasma rest frame, is equal to their ionization energy:

$$\frac{m_n V_c^2}{2} = eU_i \,. \qquad (1)$$

The CIV process has been studied in a number of laboratory experiments in different geometries, in a large number of gases and in wide ranges of gas density and magnetic field strength. These experiments are reviewed by e.g. Danielsson (1973) and Brenning (1982). The overall conclusion agrees well with Alfvén's original hypothesis: the CIV effect does definitely exist, and occurs above a threshold velocity which depends very little on the magnetic field strength and the neutral density. The threshold velocity lies typically within 50 % of the value V_c from Eq. 1, *i.e.* it is determined almost exclusively by the neutral component.

It is clear from several laboratory experiments (Danielsson and Brenning, 1975; Brenning, 1981; Venkataramani and Mattoo, 1986; Chang, 1988) that both the magnetic field strength and the neutral density must be above some lower limits, but there is still some uncertainty about the values of these limits. Papadopoulos (1982) noted that the modified two-stream instability, which was proposed by Sherman (1969) and Raadu (1978) to heat the electrons in CIV, is theoretically expected to be suppressed for $V > V_A(1 + \beta_e)$. For any given combination of plasma velocity and neutral density, this would give a lower limit to the magnetic field strength. Brenning (1985) compared this limit to all the results from impact experiment performed at that time, and found fairly good agreement. A more comprehensive study, which contains also laboratory discharge experiments, is shown in Fig. 1 (from Brenning, 1989). For strong magnetic field, defined by $V_A > 10\, V_0$, the CIV effect did always appear, and for weak magnetic fields, defined by $V_A < V_0$, the CIV effect was always absent. For intermediate magnetic field strengths the CIV effect was sometimes seen, and sometimes weak or

irreproducible. Although there is no single experiment with really good diagnostics which studies the efficiency of the CIV effect close to the threshold $V_A = V_0$, the consistency between the large number of experiments shown in Fig. 1 indicates that V_A/V_0 is indeed the relevant parameter for the magnetic field strength. Computer simulations (Machida and Goertz, 1988) also support this view.

Concerning the neutral density required for CIV there are different theoretical estimates but little done experimentally. Galeev (1981) and Formisano *et al.* (1982) proposed that efficient CIV interaction is only possible if the neutral density is so high that the ionization frequency (per electron) is higher than the gyro frequency of the ionized neutrals,

$$\frac{\nu_i}{\omega_{gi}} > 1 . \qquad (2)$$

Their argument is that the electrostatic instabilities which transfer the energy to the electrons require a beam distribution of ions in order to be efficient, and that this only is possible if the condition above is fulfilled. For lower ionization rates the ions get a gyrotropic distribution in velocity space, and the efficiency of energy transfer, which is usually denoted by η, should gradually approach a value $\eta = 0.025$ which applies for $\nu_i/\omega_{gi} < (m_e/m_i)^{1/2}$. Haerendel (1986) and Brenning (1986) argued that the situation could be different in transient experiments, provided that the instability growth rate is larger than the ion gyro frequency. In that case, a ring distribution should not have time to develop, and efficient CIV interaction could be possible for values of ν_i/ω_{gi} far below unity.

These alternative variations of η with the parameter ν_i/ω_{gi} are shown in Fig. 2 (From Brenning and Axnäs, 1988). The upper graph shows the transient situation, and the lower graph is made schematically after Galeev (1981). Machida and Goertz (1986) have made a computer simulation which is drawn by a circle in the lower graph. They followed the interaction during three ion gyro periods ($t = 20\ \omega_{gi}$) and found a constant value $\eta = 0.32$ during that time although the ionization rate was low, $\nu_i/\omega_{gi} < (m_e/m_i)^{1/2}$. This supports the opinion that in a transient situation there can be efficient CIV even if the condition (2) is not fulfilled.

The purpose of the present experiment is to study CIV interaction close to the threshold values of V_A/V_0 and ν_i/ω_{gi}. We have chosen to focus on the energy transfer factor η, because this gives the clearest measure of the efficiency of the interaction. We have made a series of

experiments with varying neutral density and magnetic field strength, and use a combination of microwave interferometry and spectroscopy to measure both the ionization rate and the changes in the high-energy electron population. These measured quantities are combined to give the η value.

2. The Experiment.

The plasma source and the diagnostics equipment is shown in Fig. 3. The plasma is generated by a plasma gun of the conical theta pinch type, which produces a hydrogen plasma stream with 10-20 μs duration, and with a velocity V_0 about 150 - 300 km/s. As neutral gas we use helium, which has a critical velocity of 35 km/s. The plasma is generated during such a short time that the plasma velocity can be approximated from the time of flight from the plasma gun, $V_0 = L/t$. This velocity agrees both with the self-polarization field $\mathbf{E_P} = - \mathbf{v_0 x B}$, which is measured by floating double probes (Brenning *et al.*, 1981b), and with measurements with an ion energy analyzer (Lindberg, 1978). At the penetration into the transverse magnetic field the plasma flattens from a circular cross section to a flat slab with approximate dimensions 0.1x0.4 m., elongated in the y direction as indicated in Fig. 3. In an earlier experiment, Brenning *et al.* (1981b) found that the electron energy distribution was strongly influenced by the penetration into the transverse magnetic field: a high-energy tail of W_e>100 eV electrons was formed, containing up to 20-25% of all electrons.

The neutral helium cloud is let in by a fast electromagnetic valve and has expanded to about 0.5 meters diameter at the time of arrival of the plasma stream. A neutral gas probe was used, prior to the plasma shots, to measure the column neutral gas density $\int n_{He} dz$ along the plasma flow to the z coordinate where the lines of sight of the interferometer and the spectrograph cross the plasma stream.

We used combination probes (Lindberg, 1976) to measure both the electric field and the density in a the plasma stream. However, it has been shown in other CIV experiments (Lehnert *et al.*, 1966) that already the presence of a very small object can have a strong effect on the plasma flow. For this reason the probes were located a distance downstream from the observation position. The probe measurements were used only to study the undisturbed plasma stream, to obtain the plasma stream profile in the x direction, and to monitor the reproducibility of the plasma gun.

The main diagnostic methods were microwave interferometry and spectroscopy, which both give integral measurements along the line of sight. Both interferometer and spectrograph were aimed at the centre of the neutral gas cloud where the lines of sight crossed as shown in Fig. 3. The interferometer is described by Brenning (1984, 1988). The interferometer detector signals were stored in a VAX 11/750 computer which calculated the phase shift, the attenuation of the transmitted beam, and the plasma (column) density $\int n_e dx(t)$ as function of time for each shot with the plasma gun. The spectrograph measured the absolute strengths $I_\lambda(t)$ of the He I line at $\lambda = 3889$ Å and the He II line at $\lambda = 4686$ Å, which also were stored in the computer.

The limits to the studied neutral gas range were determined by the reliability of the spectroscopic measurements. At high neutral and plasma densities the limit was set by the build-up of the metastable 2^3S level, which is the lower level for the 3889 Å line. A high population of the 2^3S level has two opposing effects. Imprisonment of the 3889 Å line decreases the line strength, while direct excitation by electron impact from the 2^3S level increases the line strength. We ascertained that imprisonment was negligible by use of a mirror which could be alternatively inserted or taken away as shown in Fig. 3. In the absence of imprisonment, the line strength doubles when a mirror is inserted this way. The direct excitation of the 3889 Å line from 2^3S was estimated and taken into account as described in Appendix 2. At low neutral and plasma densities, the limit to measurements was that the 4686 Å line became very weak; at the lower limits of our study we measured a few photons per μs in single-shot measurements, and had to verify the presence of the line by taking line profiles with many-shot averages.

We used four strengths of the transverse magnetic field, 0.075, 0.150, 0.225 and 0.300 T, giving values of V_A/V_0 in the range 1.1 - 4.2. For each value we varied the helium density in the range $4.9 \cdot 10^{18}$ - $2.8 \cdot 10^{20}$ m^{-3}. The experimental series covered ν_i/ω_{gi} values in the range 0.002 to 0.6.

3. Method of evaluation

The evaluation follows the block diagram in Fig. 4. The spectroscopic measurement gives the column photon excitation rate $\int I_\lambda dx(t)$ (photons per m^2 and second) along the line of sight of the spectrograph, as a function of time. The column electron density $\int n_e dx(t)$ is obtained from

the interferometer. These are our central measured quantities, but they have the disadvantage for the following discussion that they depend on the neutral density and on the plasma density. We will instead use the line excitation rate coefficients $S_\lambda = <\sigma_\lambda v_e>$, where σ_λ is the cross section for excitation of the line with wavelength λ. S_λ depends only on the electron energy distribution. It is calculated from the measured quantities by

$$S_\lambda(t) = \frac{\int I_\lambda dx(t)}{n_{He}\int n_e dx(t)} . \qquad (3)$$

When the plasma stream interacts with the neutral gas the plasma density increases rapidly in time, and the plasma stream spreads out in the x direction. Since both the spectrograph and the interferometer give column measurements along closely the same line of sight, the S_λ values are correctly calculated by Eq. 3 independent of these variations, assuming only that the electron energy distribution does not vary along the line of sight.

The two lines are excited by different parts of the electron energy population. Fig. 5 shows the helium line excitation cross sections together with the cross section for ionization of helium from the ground state (the sources for all cross sections used in this paper are found in Appendix I). The 3889 Å line is mainly excited by electrons in the 25 - 75 eV range, while the 4686 Å line has a threshold at 75.6 eV, and an excitation rate which is close to constant above 125 eV. Since the 3889 Å and 4686 Å line excitation cross sections overlap only little, and together cover the whole energy range of the ionization cross section, the measured line strengths can be combined to give the average ionization rate per electron. Using the cross sections in Fig. 5, we have derived the formula

$$\nu_i = (31\, S_{3889} + 4500\, S_{4686})\, n_{He}. \qquad (4)$$

For the calculation of the η value we will need a measure of the energy content in the high-energy electron tail ($W_e > 25$ eV). We use the approximation, in units eV/m^3:

$$W_{e,tail} = (1.5\text{x}10^{17} S_{3889} + 2.5\text{x}10^{19} S_{4686}) n_e. \qquad (5)$$

Finally it is of some interest how the high-energy tail is distributed. Using the cross sections in

Fig. 5, we have derived the following estimates of the parts of the electron population which excite the two lines. We call them population II (25 eV < W_e < 75 eV) and population III (W_e >75 eV):

$$\frac{n_{II}}{n_e} = 3.0\text{x}10^{15} S_{3889}, \tag{6}$$

and

$$\frac{n_{III}}{n_e} = 1.7\text{x}10^{17} S_{4686}. \tag{7}$$

The accuracy of relations 4-7 depends on the actual energy distribution. We have estimated the accuracy by the following procedure: for different electron energy distributions f(W_e) we have calculated $S_\lambda = \int \sigma_\lambda v_e f(W_e) dW_e$ for λ = 3889 and 4686, using the excitation cross sections shown in Fig. 5. Then we have calculated v_i, $W_{e,tail}$, n_{II}/n_e and n_{III}/n_e from these values of S_{3889} and S_{4686} and relations 4-7. Finally, we have compared these calculated values with the correct values for the energy distribution we started with. The result is that all four relations 4 - 7 are correct within 2 % if the electrons above 25 eV consist of any combination of two monoenergetic populations, one at 50 eV and one at 150 eV. If the electrons are rather evenly distributed between 25 and 300 eV, the accuracy is still rather good. The worst possible case is if the electrons are monoenergetic with energies in *one* of the ranges 25-30 eV, 70-80 eV or above 300 eV. In that case the relations 4-7 are wrong with typically a factor two. We conclude that our method of evaluation gives fairly accurate results.

4. Measurements

We will first discuss in some detail the measurements with magnetic field strength B = 0.0225 T, starting with the plasma stream without helium gas, and then pick one recording with low, one with medium and one with high helium density. This division refers to the neutral helium column density $\int n_{He} dz$ along the plasma flow to the z coordinate where the measurements were made, and reflects the expected physical processes. At *low column density*, $\int n_{He} dz < 10^{18}$ m^{-2}, the plasma stream should be uninfluenced by the presence of helium, even if a very efficient (η = 1) mechanism for CIV heating operates. At *medium column density*, $10^{18} < \int n_{He} dz < 10^{19}$, the CIV mechanism could get ignited, provided that a mechanism to feed back energy to the electrons exists. At *high column density*, $\int n_{He} dz > 10^{19}$ m^{-2}, the electron energy loss time (for inelastic collisions with neutral He) is shorter than the transit time of the plasma into the neutral

gas. Unless the CIV process is very efficient, it could therefore be damped by electron cooling.

4.1. The plasma stream without helium

Fig. 6 shows measurements in the plasma stream without helium gas, with $B = 0.0225$ T. The two top panels show the transverse electric field measured in the stream by two of the combination probes, placed 4 cm apart in the x direction. The scales to the left show the measured electric field, and the scales to the right the corresponding velocity for a self-polarized beam, where $\mathbf{E} = -\mathbf{V}\times\mathbf{B}$. The theoretical velocity calculated from time of flight from the plasma gun, $V = L/t$, is drawn by a solid line.

The measured electric field starts to rise immediately when the interferometer shows that the thin leading flank of the plasma arrives at $t = 10.5$ μs. There is a delay by 2-3 μs before the electric field reaches the self-polarization value, but this does not mean that the velocity is lower in the first arriving plasma. The time delay is of the order of the ion gyro period, and is probably associated with fringing field effects at the leading front of the plasma stream. After the initial rise, the electric field remains quite close to the expected self-polarization field, particularly during the time period 13-18 μs. We conclude that $V = L/t$ gives a good measure of the undisturbed plasma stream velocity.

The third panel in Fig. 6 shows the plasma density, measured by the microwave interferometer. The scale to the left is the measured column density (electrons/m^2) across the plasma stream. Density probe measurements (not shown here) give a plasma stream thickness of about 0.1 m, which is used to give the density scale to the right (electrons/m^3). Measurements with slower time sweeps show that the vacuum chamber is later (after 50-100 μs) filled with a stationary plasma which eventually decays on the ambipolar diffusion time. This later plasma is probably reflected off the end plate which is located 0.5 m downstream of the point of measurement. We do not know for certain when this reflected plasma population becomes disturbing at our z coordinate of measurement. However, it is probably negligible before 18 μs; only the thinner leading edge of the plasma, which arrives before 13 μs, could at that time have reached the end plate and returned to the z coordinate of the observations.

The bottom panel of Fig. 6 shows the dimensionless number V_A/V_0, calculated from the density in the third panel together with the time-of-flight velocity from the top panel. During the

time 13-18 μs V_A/V_0 is close to constant ≈ 3.

4.2. Low column density

Fig. 7 shows measurements from one shot with the lowest helium density for which the 4686 Å line was visible against the background, $n_{He} = 4.9\text{x}10^{18}$ m^{-3}, corresponding to a column density along the flow $\int n_{He} dz = 6.0\text{x}10^{17}$ m^{-2}. The top panel shows the transverse electric field measured by a combination probe, and the second panel shows the plasma density from the microwave interferometer. Both these curves are close to the results without helium gas in Fig. 6, which indicates that the the plasma stream was only little influenced by the presence of helium.

Panels 3 and 4 of Fig. 7 show the excitation rate coefficients S_{3889} and S_{4686}, calculated by Eq. 3 from the plasma density and the measured line strengths. In order to avoid divisions with values $\int n_e dz$ close to zero, the S_λ values are artificially put to zero until $\int n_e dz$ has increased to twice the noise level, which happens at $t = 11.0$ μs in this shot. The background light was investigated by measurements without helium, and by measurements 20 Å beside the line centres. The result is that the background is negligible (about 5 % of the signal) for the 3889 Å line, while there is a constant background level, independent of the presence of helium, around the 4686 Å line. The level is shown with a dashed line in panel 4. We do not know the origin; it could be reflected light from the walls, or light from impurities in the plasma stream.

The 3889 Å line strength is influenced by excitation of helium atoms that are in the metastable level 2^3S. The process is treated in Appendix II with the following result: before 13 μs, the influence of the 2^3S level is negligible, and Eq. 6 gives an accurate measure of the relative population n_{II}/n_e (electrons with energies 25 eV < W_e < 75 eV). This ratio is about 3 % at 13 μs. For times later than 13 μs, there is an increasing contribution due to excitation from the 2^3S level; after 15 μs this excitation process probably dominates the 3889 Å line. As a consequence the n_{II}/n_e values in Fig 7, after 13 μs, are upper limits to that population. Fortunately this uncertainty does only little harm to the investigation here since both the ionization and the tail electron energy are dominated by population III.

The relative population n_{III}/n_e (electron energies W_e > 75 eV) from Eq. 7 are shown by the scales to the right of panel 4. In the first arriving rather thin plasma, before 13 μs, there is an

extreme overpopulation of the high-energy electron tail reflected by n_{III}/n_e values well exceeding 50 %. The n_{III}/n_e value then decreases in time: at $t = 13$ μs, $n_{III}/n_e = 12$ % (with the background level subtracted). For the low helium density used here, the measurement of n_{III}/n_e becomes uncertain after 15 μs due to the background level.

The high values of n_{III}/n_e before 13 μs seem to be real: they are not associated with the lowest values of $\int n_e dz$, so they do not arise because of division with $\int n_e dz$ values close to zero in Eq. 3. Furthermore, they are consistently seen in all recordings with helium, while they disappear when the same evaluation is made using the background light without helium, or using the background light 20 Å beside the line centre. This high-energy electron tail has been studied in more detail by Brenning *et al.* (1981), who found that n_{III}/n_e is below 1 % in the case where the magnetic field does not curve but is maintained parallel to the plasma flow. Their conclusion was that the high-energy electron tail is produced as the plasma stream enters the curved magnetic field. The mechanism of acceleration is unknown; however, Brenning *et al.* (1981) argue that electric field components parallel to the magnetic field could arise in the transition from flow-parallel to transverse magnetic field, and that these could accelerate the electrons. The potential across the 0.1 m wide plasma stream is of the order of 500 V, which is large enough for such a process to give the observed electron energies.

Now let us make some estimates concerning the part of the plasma stream that arrives at the time $t = 13$ μs. With the background levels subtracted, we have from Fig. 7 the rate coefficients $S_{3889} = 10^{-17}$ m^{3}s^{-1} and $S_{4686} = 7\text{x}10^{-19}$ m^{3}s^{-1}. The total ionization rate up to $z = 0$ can then be found from integration of Eq. 4 along the plasma flow; we assume that, at this low helium density, the S_λ values and the velocity are constant so that they can be taken out of the integration:

$$\int_{\substack{\text{penetration}\\ \text{time}}} \nu_i\, dt = \int_{\text{to } z=0} (31 S_{3889} + 4500\, S_{4686})\, n_{He} \frac{1}{V_0}\, dz = \frac{31\, S_{3889} + 4500\, S_{4686}}{V_0} \int_{\text{to } z=0} n_{He} dz \qquad (8)$$

With $V_0 = 2.1\text{x}10^5$ ms^{-1} and $\int n_{He} dz = 6\text{x}10^{17}$ m^{-2}, the integrated ionization up to $z = 0$ is $n_{He^+}/n_e = 1$ %.

The energy content in the high-energy electron tail from Eq. 7 is

$$W_{e,tail} = 20\, n_e \qquad (9)$$

eV/m^3. About 87 % of this energy lies in population III, above 75 eV. The tail population is little influenced by the presence of the low-density helium cloud: The ionization of $n_{He^+}/n_e = 1$ % requires an amount of energy $W_{ioniz} = eU_i n_e/100 = 0.25\, n_e$, again in units eV/m^3. This energy loss is negligible compared to the total energy in the tail above. The possible energy gain through the CIV process can be calculated by the mathematical model described in section 4 and shown to be small.

We conclude that the measurements at low column density give reliable information about the undisturbed plasma stream. The electron distribution is highly non-thermal, with a large part of the electrons in the high-energy tail above 75 eV. This high-energy population is most pronounced in the leading front of the plasma stream. This electron energy distribution should favour the CIV interaction by triggering the ionization efficiently. The plasma parameters are also well suited for the investigation intended here: Eq. 4 gives an ionization rate $\nu_i/\omega_{gi} = 0.03$. This is of the order of the limit $\nu_i/\omega_{gi} = (m_e/m_i)^{1/2} = 0.012$ given by Galeev (1981) and Formisano *et al.* (1982) below which there would be very inefficient electron heating. Higher values of ν_i/ω_{gi} are easily reached in the experiments using higher helium densities. However, there is the risk that the ionization caused by these already-present energetic electrons is mistaken for CIV interaction. Such effects must be distinguished from the "real" CIV effect, which requires energy transfer to the electrons.

4.3. Medium column density

Fig. 8 shows measurements at medium column density, $\int n_{He} dz = 6.2\text{x}10^{18}$ m^{-2}. The transverse electric field E_x, is here strongly modified compared to the undisturbed plasma stream, and even becomes negative during the time 10-16 μs. The probable explanation for the change in sign is that the 0.1 m wide plasma stream is deflected a bit sideways in the interaction, so that the probe is outside the heart of the stream. Outside the main stream E_x is usually much lower than inside, and sometimes even reverses polarity.

The plasma density (panel 2 of Fig. 8) closely follows the density increase in the absence of helium during the time t = 11-14 μs. Then it builds up to, and remains at, about twice the value without helium. The measured S_{3889} is shown in panel 3. Compared to the low density case,

S_{3889} is here about 40 % higher before t = 13 μs, and about 40 % lower after t = 13 μs. The S_{4686} value finally (panel 4) is reduced by about a factor 4 compared to the low density case, but shows the same time dependence. The relative population n_{III}/n_e (electrons in the energy range above 75 eV) has a peak about n_{III}/n_e = 20 % in the front of the plasma stream, and then decreases in the later arriving plasma. During the time period 13-15 ms, $n_{III}/n_e \approx 3$ %. The background level for the 4686 Å line is much lower here than it was in the low density case.

We take measurements from the time t = 13 μs for a closer study. With the background for 4686 Å subtracted, the S_λ values in Fig. 8 are $S_{3889} = 1.1\text{x}10^{-17}$ m^3s^{-1} and $S_{4686} = 2\text{x}10^{-19}$ m^3s^{-1}. The energy content in the electron tail from Eq. 7 is

$$W_{e,tail} = 7\, n_e \qquad (11)$$

The energy in the tail has actually *decreased* from the value $W_{e.tail} = 20\, n_e$ in the undisturbed plasma stream. We can therefore estimate an upper limit to the energy transfer factor η as follows. If each ionization of helium is accompanied by an equal amount of energy loss in excitations (usually a reasonable approximation), and if a fraction η of the released energy goes to the electrons through the CIV process, then each ionization changes the total energy content in the electrons by an amount (in units eV) $\Delta W = (\eta m_{He} V^2/2 - 2eU_i)/e = (835\eta - 50)$. Although the decrease in electron energy from Eq. 9 to Eq. 11 refers to the tail electrons and not the total population, it implies a negative value of ΔW, which in turn implies

$$\eta < \frac{50}{835} = 6\%. \qquad (12)$$

Like in the preceding section, we calculate the range in v_i/ω_{gi} from Eq. 6. We use the values of S_{3889} and S_{4686} in the original plasma stream, which applies upstream of z = 0 where the stream enters the helium cloud. This gives $v_i/\omega_{gi} = 0.32$.

Now let us look at the depletion of electron populations n_{II} and n_{III}. The transit time through the helium cloud is about 1 μs. The ionization frequency for electrons in population III (energies above 75 eV) is $2.7\text{x}10^{-14}\, n_{He} = 1.4\text{x}10^6$ s^{-1}. Assuming that excitation collisions are equally frequent as ionization, the electrons in population III make on the average 3 ionization or excitation collisions during the time of transit 1 μs, losing on the average 25 eV in each collision. The net loss of electrons out of population III depends on the initial energy

distribution, which is unknown; electrons below 100 eV will be lost after one collision, while electrons with higher initial energies would need more than one collision. However it is clear that the observed decrease in population III by a factor of 4 is consistent with collisions with neutral helium.

The ionization frequency for electrons in population II is a bit lower, $\nu_i = 1.0\text{x}10^{-14}\, n_{He} = 5\text{x}10^5\ s^{-1}$. Again assuming that excitation collisions are about equally frequent, the collision time becomes equal to the transit time 1 μs. If this were the only process at work one would expect the n_{II}/n_e value to decrease from 2 % in Fig. 7 to 1 % in Fig. 8, while it in reality increases from 2 % to 3 %. However it seems likely that this could be explained by the depletion of population III during the same time period: as large part of the electrons which disappear from population III should appear in population II.

We conclude that all the observations in medium density can be understood, and support each other, without invoking the CIV effect. As an upper limit to the energy transfer efficiency we can put $\eta < 6$ % , a value which here applies for $V_A/V_0 = 3$, and $\nu_i/\omega_{gi} = 0.32$.

4.4. High column density

Fig 9 shows measurements with high column density, $\int n_{He} dz = 3.4\text{x}10^{19}\ m^{-2}$. In the centre of the cloud, the density is $n_{He} = 2.8\text{x}10^{20}\ m^{-3}$. The ionization time for electrons with energies above the ionization threshold is an order of magnitude shorter than the penetration time of the plasma to the point of observation. The depletion of the hot electrons should therefore be almost complete if there is no CIV interaction which refills the electron tail. The S_{4686} value shows that most of population III has indeed been lost: it has decreased by an order of magnitude compared to the case with medium column density. The S_{3889} value however has increased somewhat compared to the medium density case, in spite of the fact that the ionization time, also for the electrons that excite this line, is much below the penetration time. As we will discuss further in the following sections, the reason could be either that there is some CIV heating of the electrons, or that population II is replenished by the loss from population III.

4.5. Results from the whole experimental series.

Fig 10 shows results from the whole experimental series for the time $t = 13$ μs. This time is

chosen as a compromise in order to avoid the influence from the initial transient on one hand, and excitations from the metastable 2^3S level on the other. At t = 13 μs, the initial transient (with low density and extreme overpopulation of the high-energy electron tail) has passed by, and the plasma stream has entered the phase where the self-polarization field agrees with the time-of-flight velocity, **E** = -**VxB** (see Fig. 6). At the same time, the contribution to the 3889 Å line from the metastable level is still negligible (see appendix 2).

We used four magnetic field strengths (B = 0.0075 T, 0.015 T, 0.0225 T and 0.3 T) and eight neutral densities ranging from $n_{He} = 4.9\text{x}10^{18}$ m^{-3} to $n_{He} = 2.8\text{x}10^{20}$ m^{-3}. For each combination we measured both single shots and five-shot averages in order to get a view of the shot-to-shot variations. We also measured the light strength at the line centre and at a distance 20 Å from the line centre to get a measure of the background to the spectral lines, which has been subtracted in Fig. 10. Finally, we recorded the line strengths both with and without the insertable mirror shown in Fig. 3, in order to check on the effect of imprisonment on the 3889 Å line. The four magnetic field strengths correspond to the values V_A/V_0 = 1.1, 2.0, 3.0 and 4.2 written on the top of Fig. 10. The S_λ values are plotted as function of the column helium density $\int n_{He} dz$ along the plasma flow to the point of measurement at z = 0. The the scales at the bottom with the normalized ionization rates ν_i/ω_{gi} are calculated as will be described in the following section.

The S_λ values for the two weakest magnetic fields, corresponding to V_A/V_0 = 1.1 and V_A/V_0 = 2.0 in Fig. 10, show no sign of electron heating. The decay of S_{4686} with $\int n_{He} dz$ follows within the experimental error the expected depletion of population III through inelastic collisions with helium, and the S_{3889} value changes little with $\int n_{He} dz$. For the next stronger magnetic field, corresponding to V_A/V_0 = 3.0, both spectral lines are influenced at the highest neutral densities, $\int n_{He} dz > 10^{19}$ m^{-3}: S_{4686} decreases slower than for the two weaker fields indicating that the cooling through inelastic collisions is counteracted by some heating process, and S_{3889} shows an increase by about a factor two . Both these trends are much increased for the strongest magnetic field, corresponding to V_A/V_0 = 4.2. For the highest neutral densities S_{4686} is more than an order of magnitude higher than it was for V_A/V_0 = 1.1 and V_A/V_0 = 2.0, and at the same time S_{3889} reaches a maximum, which corresponds to 30 % of the electrons being in population II. This result is particularly significant since the only parameter that varies between the four columns in Fig. 10 is the magnetic field strength. The plasma stream has for all the experiments the same initial density and velocity, and start into the neutral cloud with

close to the same S_{3889} and S_{4686} values. Consequently it is clear the electron heating increases dramatically from the weaker magnetic fields where V_A/V_G= 1-2 to the strongest magnetic field where V_A/V_0 = 4.2, and also that there is a lower limit to the neutral density. For a quantitative interpretation of Fig. 10 in terms of η values we have developed the mathematical model in the following section.

5. A Mathematical Model of the Interaction

The model uses as input parameters the values of S_{3889}, S_{4686}, n_{He}, n_e and V measured at low column density and then follows the ionization, the change in velocity, and the electron tail population as function of the column density $\int n_{He} dz$ along the flow into the neutral cloud. The electrons (density n_e) are divided into three populations: a cold population I, below 25 eV ($n_{e,I}$), a population II consisting of the electrons in the range 25-75 eV ($n_{e,II}$) which excites mainly the 3889 Å line, and a population III above 75 eV ($n_{e,III}$) which excites the 4686 Å line. The rate coefficients $<\sigma v_e>$ for line excitation and ionization for these populations are chosen so that they agree with Eq:s 4-7. A factor η of the energy $m_{He}V^2/2$ released in each ionization or charge exchange collision is divided between the two hot populations so that a fraction κ goes to population II and a fraction (1-κ) to population III. The hot populations are depleted through ionization and line excitation; electrons which are lost from population III are added to population II. The electrons lost from population II are added to the cold population I.

The ions consist of the hydrogen ions in the original plasma stream (density n_{H^+}) and the helium ions (density n_{He^+}) created through electron impact ionization. Elastic momentum transfer and charge transfer collisions between H^+ ions and He atoms have small cross sections and are neglected, while the resonant charge transfer collisions between He^+ ions and He atoms have very large cross sections are included. The ions are assumed to be cold and hence pressure gradients are neglected.

The one-dimensional rate equations in the flow direction (z) are if all charged particles have the same flow velocity $V(t,z)$:

$$\frac{\partial n_e}{\partial t} + \frac{\partial}{\partial z}(n_e V) = n_{He}\left(n_{e,III} < \sigma V_e >_{i,III} + n_{e,II} < \sigma V_e >_{i,II} \right) \qquad (13)$$

$$\frac{\partial n_{He^+}}{\partial t} + \frac{\partial}{\partial z}(n_{He^+} V) = n_{He}(n_{e,III} \langle \sigma V_e \rangle_{i,III} + n_{e,II} \langle \sigma V_e \rangle_{e,II}) \quad (14)$$

$$\frac{\partial n_{H^+}}{\partial t} + \frac{\partial}{\partial z}(n_{H^+} V) = 0 \quad (15)$$

$$\frac{\partial n_{e,III}}{\partial t} + \frac{\partial}{\partial z}(n_{e,III} V) = - n_{He} n_{e,III} \langle \sigma V_e \rangle_{loss,III} +$$

$$\eta n_{He} \left(n_{e,II} \langle \sigma V_e \rangle_{i,II} + n_{e,III} \langle \sigma V_e \rangle_{i,III} + n_{He^+} (\sigma_{ch.tr} V) \right) \frac{m_{He} V^2}{2W_{III}} (1-\kappa) \quad (16)$$

$$\frac{\partial n_{e,II}}{\partial t} + \frac{\partial}{\partial z}(n_{e,II} V) = n_{He}(- n_{e,II} \langle \sigma V_e \rangle_{loss,II} + n_{eIII} \langle \sigma V_e \rangle_{loss,III}) +$$

$$\eta n_{He} \left(n_{e,II} \langle \sigma V_e \rangle_{i,II} + n_{e,III} \langle \sigma V_e \rangle_{i,III} + n_{He^+} (\sigma_{ch.tr.} V) \right) \frac{m_{He} V^2}{2W_{II}} \kappa \quad (17)$$

$$n_{H^+} + n_{He^+} = n_e \quad (18)$$

The momentum equation is:

$$\frac{\partial}{\partial t}[(n_{H^+} m_{H^+} + n_{He^+} m_{He^+}) V] + \frac{\partial}{\partial z}[(n_{H^+} m_{H^+} + n_{He^+} m_{He^+}) V^2)] =$$

$$= - n_{He} n_{He^+} \sigma_{ch.tr.} m_{He^+} V^2 \quad (19)$$

For a comparison between the model and the measurements use the fact that, for all four values of V_A/V_0, the measured S_{4686} and S_{3889} in Fig. 10 are close to the same at the column density $\int n_{He} dz = 2 \times 10^{18}$ m^{-3}. By starting at that column density we can therefore make one model calculation which is relevant for all the experiments. We have done that, and solved the steady-state case ($\partial/\partial t = 0$) of Eq:s 13 - 19 by iteration forward in column density until both population II and population III are completely depleted by inelastic collisions. This calculation

was made for energy transfer factors $\eta = 0$, 0.1, 0.2, 0.3, 0.4 and 0.5, but only for one value of $\kappa = 0.5$. $\kappa = 0.5$ means that the energy which is transferred to the high-energy electron population is equally divided between populations II and III. Finally we calculated S_{3889} and S_{4686} from

$$S_{3889} = \langle \sigma V_e \rangle_{3889,II} \frac{n_{e,II}}{n_e} \tag{20}$$

and

$$S_{4686} = \langle \sigma V_e \rangle_{4686,III} \frac{n_{e,III}}{n_e} \tag{21}$$

The result is shown in Fig. 11. Let us first compare model and experimental results corresponding to the absence of CIV interaction. The model (Fig. 11, $\eta = 0$) and the measurements (Fig. 10, $V_A/V_0 = 1.1$ and $V_A/V_0 = 2.0$) agree well in the sense that S_{3889} remains close to constant over an order of magnitude in $\int n_{He} dz$, while S_{4686} drops by a factor of 50 over the same range in column density. For the next stronger magnetic field (Fig. 10, $V_A/V_0 = 3.0$), S_{3889} increases by a factor of two for the highest column densities while S_{4686}, also for the highest column densities, becomes 3 times larger than it was for the weaker field. The closest match in the model calculation is $\eta \approx 0.1$. The strongest magnetic field finally (Fig. 10, $V_A/V_0 = 4.2$) corresponds best to the model calculation using $\eta \approx 0.3$.

The only significant difference between the model and the experimental results is that the model S_λ values in Fig. 11 consistently correspond to values of $\int n_{He} dz$ that are a factor 3 below the experimental $\int n_{He} dz$ in Fig 10. There are several possible explanations for this discrepancy: the model contains several cross sections, each with its own uncertainty. Also, the division of energy between populations II and III, determined by the κ parameter in Eq:s 16 and 17, is unknown as well as the exact energy distribution of the electrons that excite the lines. We have made a number of calculations varying these uncertain parameters and found that we can change the line strengths by up to a a factor two, and increase the penetration depth by typically a factor 2-3. For all these calculations, however, the main conclusions hold: with a scale factor in front of $\int n_{He} dz$ as the only uncertain, the model can reproduce all the observations in Fig. 10. For all the calculations, the increased line strengths observed for $V_A/V_0 = 3.0$ and $V_A/V_0 = 4.2$ correspond to energy transfer factors about $\eta \approx 0.1$ and $\eta \approx 0.3$, respectively.

We have also used the model to calculate the v_i/ω_{gi} scales at the bottom of Fig. 10. These

scales are constructed with the purpose to determine the minimum values of v_i/ω_{gi} that can trigger the CIV process. In a preliminary report of these experiments (Axnäs and Brenning, 1988) we used the actual value of v_i/ω_{gi} that was observed at $z = 0$. We now consider that this is not the relevant value. For example, assume that the CIV process has been triggered upstream of $z = 0$. Then the observed value at $z = 0$ then corresponds to a running CIV interaction, and v_i/ω_{gi} can be much larger than it was where the process was triggered. Also the opposite situation is possible: if the CIV effect has failed to trigger, the electron population can be cooled by inelastic collisions before it reaches $z = 0$, and the observed value of v_i/ω_{gi} can be far below the initial value which failed to trigger the process.

Therefore we have used the model to calculate v_i/ω_{gi} during the penetration into the neutral cloud in the absence of the CIV effect, using $\eta = 0$. The scale of v_i/ω_{gi} in Fig. 10 shows, for each column density on the scale above, the highest v_i/ω_{gi} value that was obtained during the penetration into the neutral gas cloud.

6. Summary

We have made a set of experiments to determine how the efficiency of the CIV process varies with the two dimensionless variables v_i/ω_{gi} and V_A/V_0, which have earlier been proposed on theoretical grounds to be relevant parameters for the neutral gas density and the magnetic field strength (Galeev, 1981; Formisano *et al.*, 1982; Papadopoulos, 1982.; Machida and Goertz, 1988; Haerendel, 1986, and Brenning, 1985, 1986). The strength of the CIV process is measured by the efficiency factor η of energy transfer to the electrons; this energy transfer is the central process in all theories for CIV interaction. Fig. 12 summarizes our experimental results together with the results from two earlier impact experiments. In the present experiments which are denoted by (b), CIV interaction is confirmed with an efficiency $\eta \approx 0.3$ for the parameter combination $v_i/\omega_{gi} = 0.15$, $V_A/V_0 = 4$. There is also a region with weaker interaction, $\eta \approx 0.1$, and one region where there is an upper limit, $\eta < 0.06$. The last region corresponds to experiments where the energy content in the electron tail (above 25 eV) decreased measurably with increasing neutral density, as discussed in section 4.3. The experiments with lowest neutral densities, where we can not measure the changes in the electron energy accurately enough to calculate a η value, are not included.

The region (a) in Fig. 12 shows the experiments by Danielsson (1972) and Danielsson and

Brenning (1975). Also in these experiments, a hydrogen plasma was shot at a neutral helium cloud. The main differences compared to the present experiment were that they had a stronger magnetic field (B = 0.18 T), a thinner plasma ($n_e = 3\text{x}10^{17}$ m^{-3}) and a smaller and denser helium cloud (radius 0.025 m). In their experiment, $V_A/V_0 \approx 19$. For a calculation of v_i/ω_{gi} we need a value for the electron temperature before the interaction. Danielsson and Brenning (1975) only give and upper limit, $kT_{e0} < 20$ eV, which corresponds to a value of $v_i/\omega_{gi} < 0.2$. It can be objected that this value rests on the assumption by Danielsson and Brenning (1975) that the electrons initially have a thermal distribution. However, definite upper limit is given by the final measured electron energy of 100 eV. Given the neutral density of the experiment, the ionization rate can never get much higher, independent of the electron energy. With this limit we obtain $v_i/\omega_{gi} < 0.7$. The η value in this experiment has been estimated (Brenning, 1982) to be η = 0.17 - 0.7, *i.e.*, the CIV effect was definitely operating. Region (c) in Fig. 12 is from an experiment by Brenning (1981b) with magnetic field strength B = 0.15 T and plasma density $n_e = 2\text{x}10^{18}$ m^{-3}. In this experiment a clear absence of the CIV effect ($\eta \approx 0.01$) was reported.

The results from these three experiments mutually support each other and show that the limits to the magnetic field strength and the neutral density lie in the range where they have earlier been proposed to lie on theoretical grounds. For a relatively strong magnetic field corresponding to $V_A/V_0 \approx 4$, it is possible to trigger the CIV process even for such a low initial ionization rate as $v_i/\omega_{gi} \approx 0.1$. This supports the view of Haerendel (1986) and Brenning (1986) against that of Galeev (1981) and Formisano *et al.* (1982) who put $v_i/\omega_{gi} = 1$ as the lower limit. For weaker magnetic field ($V_A/V_0 \approx 1$), the CIV effect is absent in spite of the much higher initial ionization rate $v_i/\omega_{gi} = 0.6$, in agreement the view (Papadopoulos, 1982) that the CIV process requires a subalfvénic flow.

Acknowledgements

This work has been financed by the Swedish Natural Science Research Council.

Appendix 1: cross sections.

The evaluation of absolute line strengths must be done with care in a plasma, where excitation transfer between close-lying levels can influence the apparent line excitation cross section. We will here briefly discuss these problems concerning the two lines we use here, He I 3889 Å (3^3P -> 2^3S) and He II 4686 Å (n=4 -> n=3), and also give the cross sections for the other collisional processes.

1. Excitation of the 4686 Å line.

The cross section for excitation of the 4686 Å line is taken from Hughes and Weaver (1964) who measured the cross section in a collision chamber. In a plasma, the n=4 level is degenerated, and the S, P, D and F states are populated according to their statistical weight, with respectively 1/16, 3/16, 5/16 and 7/16 of the total n=4 population. In the measurement of Hughes and Weaver (1964), the relative population of the different n=4 levels is unknown. What follows is an estimate of how much this uncertainty will influence our result. Following the treatment of Hughes and Weaver (1964) we normalize the cross sections to the σ_{4P} cross section: $\sigma_{4S} = R_1\sigma_{4P}$; $\sigma_{4D} = R_2\sigma_{4P}$, and $\sigma_{4F} = R_3\sigma_{4P}$. The total cross section of the n=4 level is then

$$\sigma_{n=4} = \sigma_{4P}(1 + R_1 + R_2 + R_3) \qquad \text{(I)}$$

The cross section for excitation of the 4686 Å line in the collision chamber is

$$\sigma_{4->3} = \sigma_{4P}\{R_1T_{4S}A_1 + T_{4P}(A_2+A_3) + R_2T_{4D}A_4 + R_3\}, \qquad \text{(II)}$$

where T_{4S}, T_{4P} and T_{4D} are the level lifetimes, and A_1, A_2, A_3 and A_4 are the transition probabilities for the 4S->3P, 4P->3S, 4P->3D and 4D->3P transitions, respectively. In a plasma, where the levels are degenerated, the line excitation cross section is

$$\sigma_{4->3\,(DEG)} = \sigma_{n=4}\ T_{DEG.}\left(\frac{A_1}{16} + \frac{3(A_2+A_3)}{16} + \frac{5A_4}{16} + \frac{7A_5}{16}\right). \qquad \text{(III)}$$

A_5 is the transition probability of the 4F->3D transition, and T_{DEG} is the lifetime of the degenerated level,

$$T_{DEG} = \left(\frac{1}{16T_{4S}} + \frac{3}{16T_{4P}} + \frac{5}{16T_{4D}} + \frac{7}{16T_{4F}}\right)^{-1} . \qquad \text{(IV)}$$

Hydrogen lifetimes and transition probabilities are sufficient here since the products of these quantities are used in the calculations. The change in 4686 Å line excitation cross section due to degeneration of the n=4 levels is a factor

$$\frac{\sigma_{4->3\,(DEG)}}{\sigma_{4->3}} = \frac{0.298\,(1 + R_1 + R_2 + R_3)}{0.41R_1 + 0.041 + 0.256R_2 + R_3} . \qquad \text{(V)}$$

A theoretical calculation by Dalgarno and McDowell (1936) puts R_2 in the range 0.20-0.25. Since the excitation to 4P is optically allowed while the transitions to 4S and 4F are forbidden, it seems safe to assume both $R_1<1$ and $R_3<1$. Putting $R_1 = 1$, $R_2 = 0.2$ and $R_3 = 1$ in Eq. (V) gives a factor 1.27; $R_1 = R_2 = R_3 = 0.2$ gives a factor 0.64. We expect the real value to lie somewhere between these extremes, i.e., not too far from 1. Our conclusion is that the degeneration of the n=4 level introduces no large error in our evaluation of the 4686 Å line.

2. Excitation of the 3889 Å line.

The $\lambda = 3889$ Å line ($3^3P->2^3S$) has been measured by several authors with general agreement concerning the maximum of the cross section, and the shape between 35 and 100 eV. We have used the measurements of St John *et al.* (1964) in this energy range. The energy dependence between threshold (23 eV) and 35 eV we have taken from Smit *et al.* (1963), while the cross section for energies above 100 eV is taken from Showalter and Kay (1975).

The 3889 Å line is, in a plasma, influenced by a mechanism related to degeneration of the upper level. Excitation transfer collisions redistributes the populations between levels which have the same main quantum numbers so that, for high plasma densities, all groups of such levels approach the statistical relative population (Brenning, 1978). The effect on several He I line excitation cross sections was studied by Brenning (1980a, 1980b) who concluded that the 3889 Å line is unique among the stronger He I lines: the apparent cross section varies only slowly with the plasma density, and this variation can be taken into account as described by Brenning (1980b).

The interpretation of the 3889 Å line is also complicated by the fact that the lower level 2^3S is metastable. This is discussed in Appendix 2.

3. Momentum loss for H^+ in He.

The stopping of the primary H^+ ions in the He gas through binary collisions is characterized by the momentum transfer collision cross section. For the proton energies of interest here (230 eV) the momentum transfer cross section is much smaller than the total elastic collision cross section. The reason is that the differential cross section has a pronounced peak in the forward direction i. e. for small scattering angles Θ and since the momentum cross section contains a extra factor (1- cosΘ) in the integrand the integral will be smaller. Thus the more easily available elastic collision cross section is not possible to use here. The momentum transfer cross section for H^+ - He collisions could be deduced from the interaction potential given by Löster (1971). For 230 eV protons $\sigma_{m.t.} = 3\text{x}10^{-22}$ m^2.

4. Electron energy loss by inelastic collisions with He.

The electron energy loss is mainly due to excitation and ionization of the He atoms. Excitation cross sections from the ground level to 2^1S, 2^1P and 2^3P levels are taken from Allen (1955) and the excitation cross section to the 2^3S level from Scott and McDowell (1975). Excitation cross sections to the 3^1P, 4^1P, 3^1S, 4^1S, 3^3P, 4^3P, 3^3S and 4^3S levels are taken from St. John *et al.* (1964). The energy dependence of the 2^1S, 2^1P and 2^3P levels is assumed to be the same as that given by St. John et al. (1964) for 3^1S, 3^1P and 3^3P levels respectively. The ionization cross section is given by Rapp and Englander-Golden (1965).

5.Charge exchange collisions

The cross section for the reactions

$$H^+ + He \rightarrow H + He^+ \qquad \sigma = 2\text{x}10^{-22}\ \text{m}^2$$

and

$$He^+ + He \rightarrow He + He^+ \qquad \sigma = 1\text{x}10^{-19}\ \text{m}^2$$

are given by Jones (1977).

6. Proton ionization of He

The cross section of the reaction

$$H^+ + He \rightarrow He^+ + e^- + H^+$$

has been given by Gilbody and Hasted (1957) for proton energies above 400 eV. The ionization cross section for 400 eV protons is slightly less than 5×10^{-23} m^2 and for 230 eV protons the cross section must be much smaller than that value.

Appendix 2: influence of 2^3S on the 3889 Å line

During the course of a plasma shot, the metastable population n_{2^3S} builds up in time. The equilibrium value of n_{2^3S}/n_{He} depends only on the electron energy distribution and is reached with a time constant t_{eq} that is independent of the helium density and inversely proportional to the plasma density. For $n_e = 10^{18}$ m^{-3} and $kT_e = 10$ eV, t_{eq} is about 10 µs. The 2^3S excitation cross section has close to the same energy dependence as the 3889 Å line; therefore the build-up (before equilibrium) of the metastable density can in our experiment be quite accurately estimated from the observed 3889 Å line strength by

$$n_{2^3S} = \int \frac{\sigma_{2^3S}}{\sigma_{3889}} I_{3889}\, dt. \qquad \text{(VI)}$$

As soon as the equilibrium density is approached, n_{2^3S}/n_{He} becomes much more uncertain since it depends strongly on the (unknown) electron energy distribution below 25 eV. For thermal electrons with kT_e between 5 eV and 100 eV, it lies in the range $10^{-3} < n_{2^3S}/n_{He} < 10^{-2}$ (Brenning, 1981a).

In our experiment, the 2^3S population influences the 3889 Å line strength by two different processes: first, direct excitation from 2^3S which increases the line strength and, second, imprisonment of the 3889 Å line which decreases the line strength.

1.Excitation of 3889 from the metastable level.

When the relative population population n_{2^3S}/n_{He} is in equilibrium, typically 80 % of the 3889 Å line intensity in a thermal plasma is due to excitations from the metastable level (Brenning, 1980b). In our plasma stream, this excitation process is highly uncertain mainly due to the unknown electron energy distribution below 25 eV. Therefore, the 3889 Å line can only be used for reliable deductions about the electron energy in the early build-up phase, when the excitation from 2^3S is small.

The ratio (3889 Å excitations from 2^3S)/(3889 Å excitations from the ground state) is independent of the helium density, and is the same in all experiments with common plasma stream temperature and density. We use the plasma density from Fig. 7 and the cross sections from Appendix 1 and Brenning (1980b). Eq. VI gives for the time $t = 13$ μs approximately $n_{2^3S} = 5 \cdot 10^{15}$ m^{-3}, a factor 10^{-4} below the density of helium in the ground state. The excitation rate of the 3889 Å line (from 2^3S) becomes about $8 \cdot 10^{19}$ m^{3}s^{-1}. This is significantly below the observed total excitation rate $5.1 \cdot 10^{20}$ m^{3}s^{-1}. We conclude that excitations from 2^3S are negligible before 13 μs. A similar calculation shows that excitations from 2^3S begin to dominate after 15 μs.

2.Imprisonment of the 3889 Å line

2^3S is the lower level of the 3889 Å line, and therefore imprisonment of the 3889 Å line (Brenning, 1981a), decreases the line strength by a factor

$$g = \frac{1}{\sqrt{\pi}\ \tau_0} \int [\ 1 - \exp\{\ -\tau_0 \exp(-x^2)\}\ ]\, dx, \qquad \text{(VII)}$$

where x is the distance from the wavelength centre normalized to the Doppler width, $\Delta\lambda_D = \nu_0(2kT/mc)^{1/2}$. τ_0 is the optical depth at the line centre which for the 3889 Å line (Brenning, 1981a) which is given by

$$\tau_0 = \frac{5.2\ 10^{-16}}{\sqrt{T_{He}}} \int n_{2^3S}\, dx\,. \qquad \text{(VIII)}$$

In the low neutral density case treated above, where $n_{2^3S} = 5 \cdot 10^{15}$ m^{-3}, the optical depth is only

0.02, and the effect of imprisonment is negligible. Even at the highest helium densities used in these experiments, imprisonment would reduce the line strength by only 10 - 20 %. We have checked this experimentally by use of an insertable mirror in the light path as described in section 2. We therefore need to make no corrections for imprisonment.

References

Alfvén, H., 1942, *On the Cosmogony of the Solar System,* Stockholms Observatoriums Annaler, **14**.

Alfvén, H., 1954, *On the Origin of the Solar System,* Oxford Clarendon Press, London.

Allen, C.W., 1955, *Astrophysical Quantities,* University o London, The Athlone Press.

Axnäs, I., and Brenning, N, 1988: *Experiments on the Magnetic Field and Neutral Density Limits on CIV Interaction*, TRITA-EPP-88-08, Royal Institute of Technology, Stockholm, Sweden (also Adv. Space Res., **Vol. 10**, n:o 7, p. 27, 1990).

Brenning, N., 1978, *'Horizontal' Thermal Equilibrium due to Excitation Transfer between Excited States of Neutral He in Transient Plasma,* J. Phys. B: Atom. Molec. Phys. **11**, L353.

Brenning, N., 1980a, *Electron Temperature Measurements in Low-Density Plasmas by Helium Spectroscopy,* J. Quant. Spectrosc. Radiat. Transfer **24**, 293-318.

Brenning, N., 1980b, *Electron Temperature Determination in Low-Density Plasmas from the He I 3889 Å and 5016 Å Line Intensities,* J. Phys. D: Appl. Phys., **13**, 1459-75.

Brenning, N., 1981a, *An appendix to the paper 'Electron Temperature Determination in Low-Density Plasmas from the He I 3889 Å and 5016 Å Line Intensities'*, TRITA-EPP-81-03, Royal Institute of Technology, Stockholm, Sweden

Brenning, N, 1981b, *Experiments on the Critical Ionization Velocity Interaction in Weak Magnetic Fields,* Plasma Physics **23**, 967-977

Brenning, N., 1982, *Review of Impact Experiments on the Critical Ionization Velocity,* TRITA-EPP-82-14, Royal Institute of Technology, Stockholm, Sweden.

Brenning, N., 1984, *An improved Microwave Interferometer Technique for Plasma Density Measurements*, J. Phys. E: Sci. Instrum., **17**, 1018.

Brenning, N., 1985, *Limits on the Magnetic Field Strength for Critical Ionization Velocity Interaction*, Phys. Fluids, **28**, 3424.

Brenning, N., 1986, *On the role of the Ionization Frequency to Gyrofrequency in Critical Ionization Velocity Interaction*, TRITA-EPP-86-10, Roya Institute of Technology,

Stockholm, Sweden.

Brenning, N., 1988, *An Improved Microwave Interferometer Technique for Plasma Density Measurements II*, J. Phys. E: Sci. Instrum., **21**, 578.

Brenning, N., 1989, *Review of the CIV Phenomenon*, manuscript in preparation.

Brenning, N., and Axnäs, I., 1988, *Critical Ionization Velocity Interaction: some Unsolved Problems*, Astrophys. and Space Science **144**, 15-30.

Brenning, N., Lindberg, L. and Eriksson, A., 1981, *Energization of Electrons in a Plasma Beam Entering a Curved Magnetic Field*, Plasma Physics, **23**, 559.

Chang, T.-F. 1988, *Laboratory Simulations of the Solar Wind-Comet Interactions*, Report UCR/IGPP-88/37, Dept. of Physics, Inst of Geophys. and Planet. Physics, Univ. of California, Riverside.

Dalgarno, A. and McDowell, M. R. C. 1936, in *The Airglow and the Aurorae*, edited by E. B. Armstrong and A. Dalgarno (Pergamon Press Inc., New York, 1936), p. 340.

Danielsson, L., 1972, *Experiments on the Interaction between a Plasma and a Neutral Gas*, Phys. Fluids **13**, 2288.

Danielsson, L., 1973, *Review of the Critical Velocity of Gas-Plasma Interaction I; Experimental Observations*, Astrophys. Space Sci. **24**, 459-485.

Danielsson, L., and Brenning, N., 1975, *Experiments on the Interaction between a Plasma and a Neutral Gas II*, Phys. Fluids **18**, 661-671.

Formisano, V., Galeev, A. A., and Sagdeev, R. Z., 1982, *The Role of the Critical Ionization Velocity Phenomenon in the Production of Inner Coma Cometary Plasma*, Planetary and Space Sci., **30**, 491.

Galeev, A. A., 1981, *Weak Turbulence Theory of an Enhanced Gas Ionization by the Plasma Flow* , Proceedings of an International School and Workshop on Plasma Astrophysics, Varenna, Italy, 27/8 - 7/9 1981 (ESA SP-161).

Gilbody, H. B. and Hasted, J.B., 1957, *Ionization by Positive Ions*, Proc. Roy. Soc. (London), **A240**, 382.

Haerendel, G., 1986, private communication.

Hughes, R. H., and Weaver, L. D., (1964), *Excitation of the He II λ4686 Å Line by Electron Impact*, Physical Review **132**, nr 2, 710.

Jones, E. M., 1977, *Atomic Collision Processes in Plasma Physics Experiments: Analytic Expressions for Selected Cross-Sections and Maxwellian Rate Coefficients II*, CLM-R 175, Culham Laboratory, Abingdon, Oxon. OX14 3DB, U.K.

Lehnert, B., Bergström, J., and Holmberg, S., 1966, *Critical Velocity of a Rotating Plasma*,

Nuclear Fusion **6**, 231-238.

Lindberg, L., 1976, *Injection of a Plasma into a Transverse Magnetic Field,* TRITA-EPP-76-10, Dept. of Plasma Physics, Royal Institute of Technology, S-100 44 Stockholm, Sweden.

Lindberg, L., 1978, *Plasma Flow in a Curved Magnetic Field,* Astroph. Space Sci. **55**, 203.

Löster, W., 1971, *Differential Cross Section Measurements for Large Angle Collisions of Protons with Atoms and Determination of the Interaction Potentials,* Abstr. VIIth Int. Conf. on the Physics of Electronic and Atomic Collisions, Amsterdam,The Netherlands, 26-30 July, p. 274.

Machida, S., and Goertz, C. K., 1986, *A Simulation Study of the Critical Ionization Velocity Process*, JGR **91**, 11965 - 76.

Machida, S., and Goertz, C. K., 1988, *The Electromagnetic Effects on the Critical Ionization Velocity Process*, JGR **93**, 11 495 - 11 506.

Papadopoulos, K.: 1982, *Electron and Ion Driven Discharges with Collective Dissipation,* Proc.'Workshop on Alfvén's Critical Velocity Effect', Max-Planck-Institut für Extra-terrestriche Physik, Garching, October 11-13, 1982.

Raadu, M. A., 1978, *The Role of Electrostatic Instabilities in the Critical Ionization Velocity Mechanism,* Astrophys. Space Sci., **55**, 125-138.

Rapp, D. and Englander-Golden, P., 1965, *Total Cross Sections for Ionization and Attachment in Gases by Electron Impact. 1 -Positive Ionization.* J. Chem. Phys. **43**, 1464.

Scott, T. and McDowell, M. R. C., 1975, *Electron Impact Excitation of n^1S and n^3S States of He at Intermediate Energies,* J.Phys. B.: Atom.. Molec. Phys. **8**, 1851.

Sherman, J. C., 1969, *Some Theoretical Aspects of the Interaction between a Plasma Stream and a Plasma in a Magnetic Field,* TRITA-EPP-69-29, Royal Institute of Technology, Stockholm, Sweden.

Showalter, J. G. and Kay, R. B., 1975, *Absolute Measurement of Total Electron-Impact Cross Sections to Singlet and Triplet Levels in Helium,* Phys. Rev. A, **11**, nr 6, 1899-1910

Smit, C., Heideman, H. G. M., and Smit, J. A., 1963, *Relative Optical Excitation Functions of Helium (Excitation by Electrons),* Physica **29**, 245-256.

St John, R. M., Miller, F. L., and Lin, C. C., 1964, *Absolute Excitation Cross Sections of Helium,* Phys. Rev. **134**, nr 4A, A888.

Venkataramani, N., and Mattoo, S. K., 1986, *Space Charge Sheath in Plasma-Neutral Gas Interaction*, Astrophysics and Space Science **121**, 83-103.

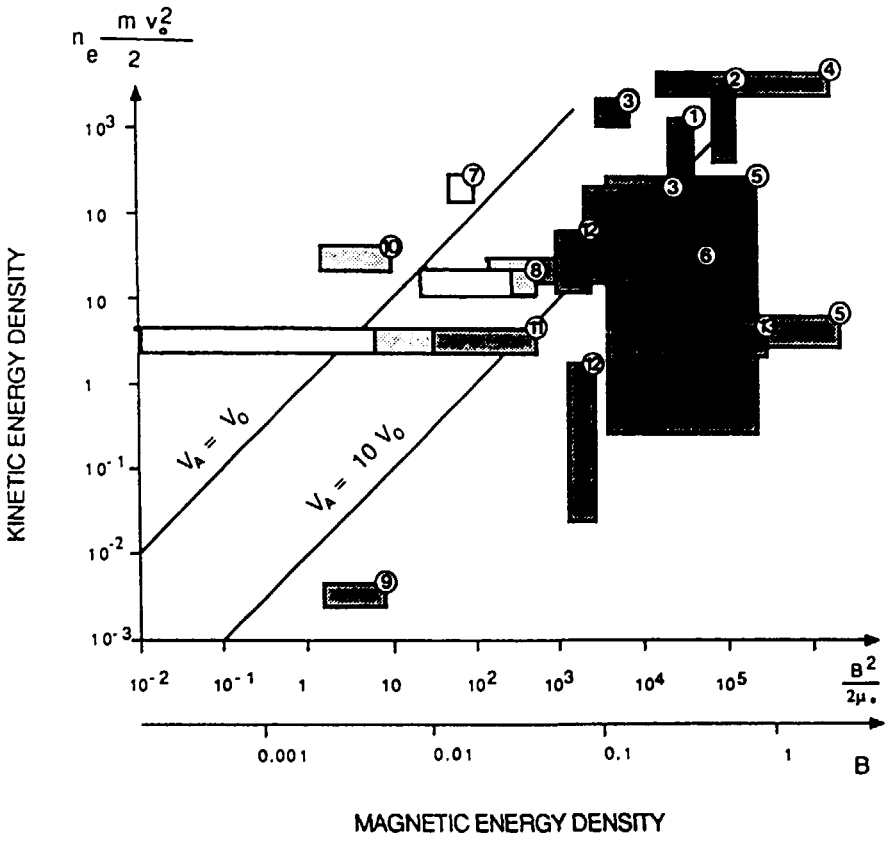

Fig. 1. Results from 13 different laboratory experiments on CIV interaction. In regions where CIV interaction is clearly confirmed, the boxes are shaded dark, and in regions where it is weak, irreproducible or otherwise uncertain they are shaded light. The blank parts of the boxes are regions of confirmed absence of CIV interaction (from Brenning, 1989).

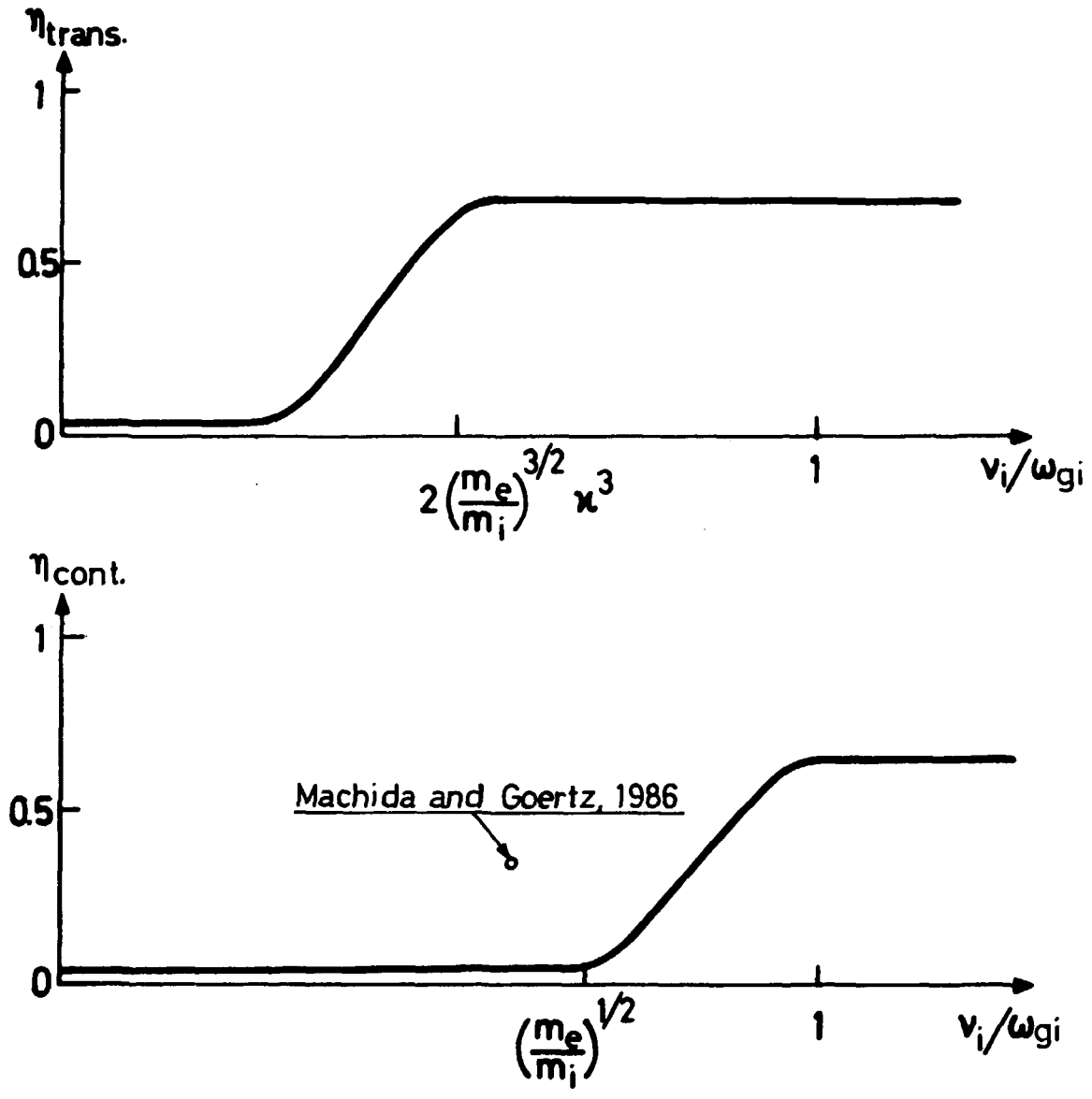

Fig. 2. The variation of the energy transfer efficiency η with ν_i/ω_{gi} (from Axnäs and Brenning, 1988). The upper graph shows the initial state of a transient situation, and the lower shows a homogeneous steady state situation (drawn schematically after Galeev, 1981). The circle in the lower graph shows the result of a computer simulation for a case in between transient and steady state.

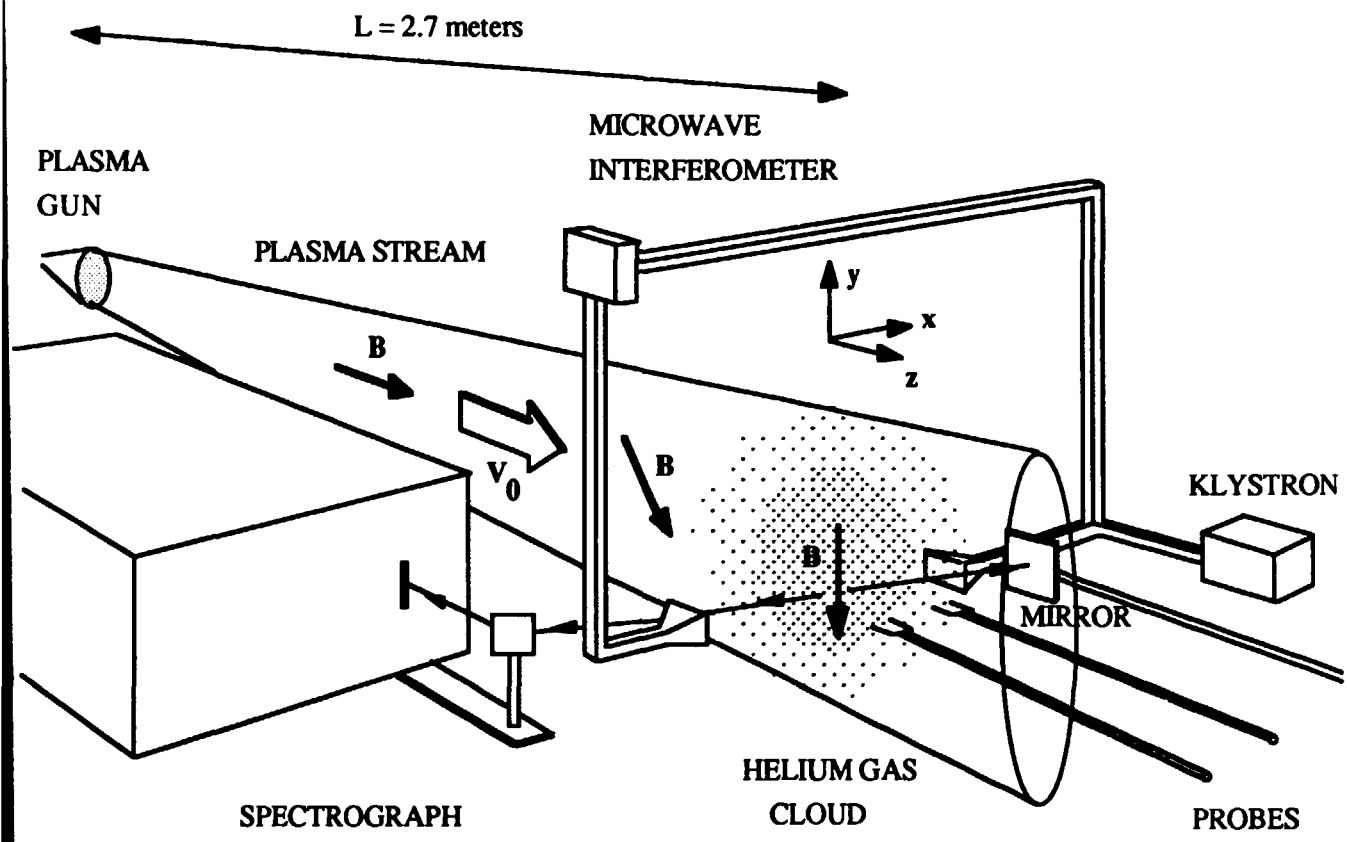

Fig. 3. The plasma source and the diagnostics equipment.

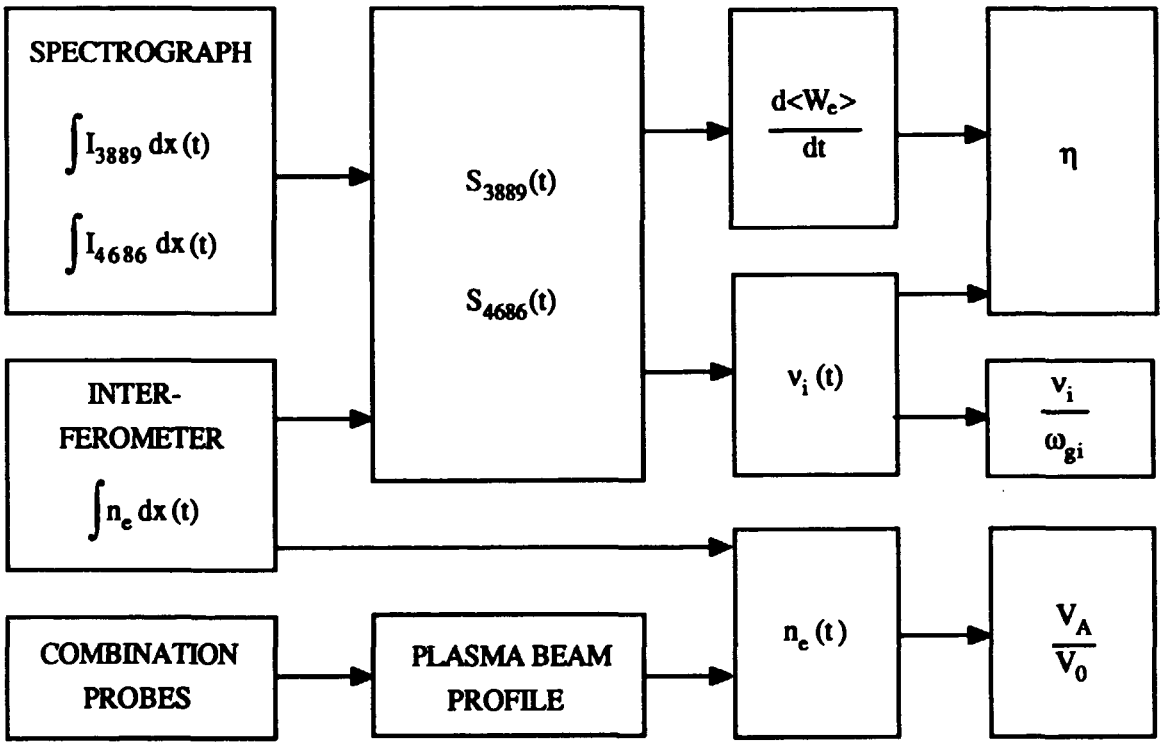

Fig. 4. Evaluation of the measurements.

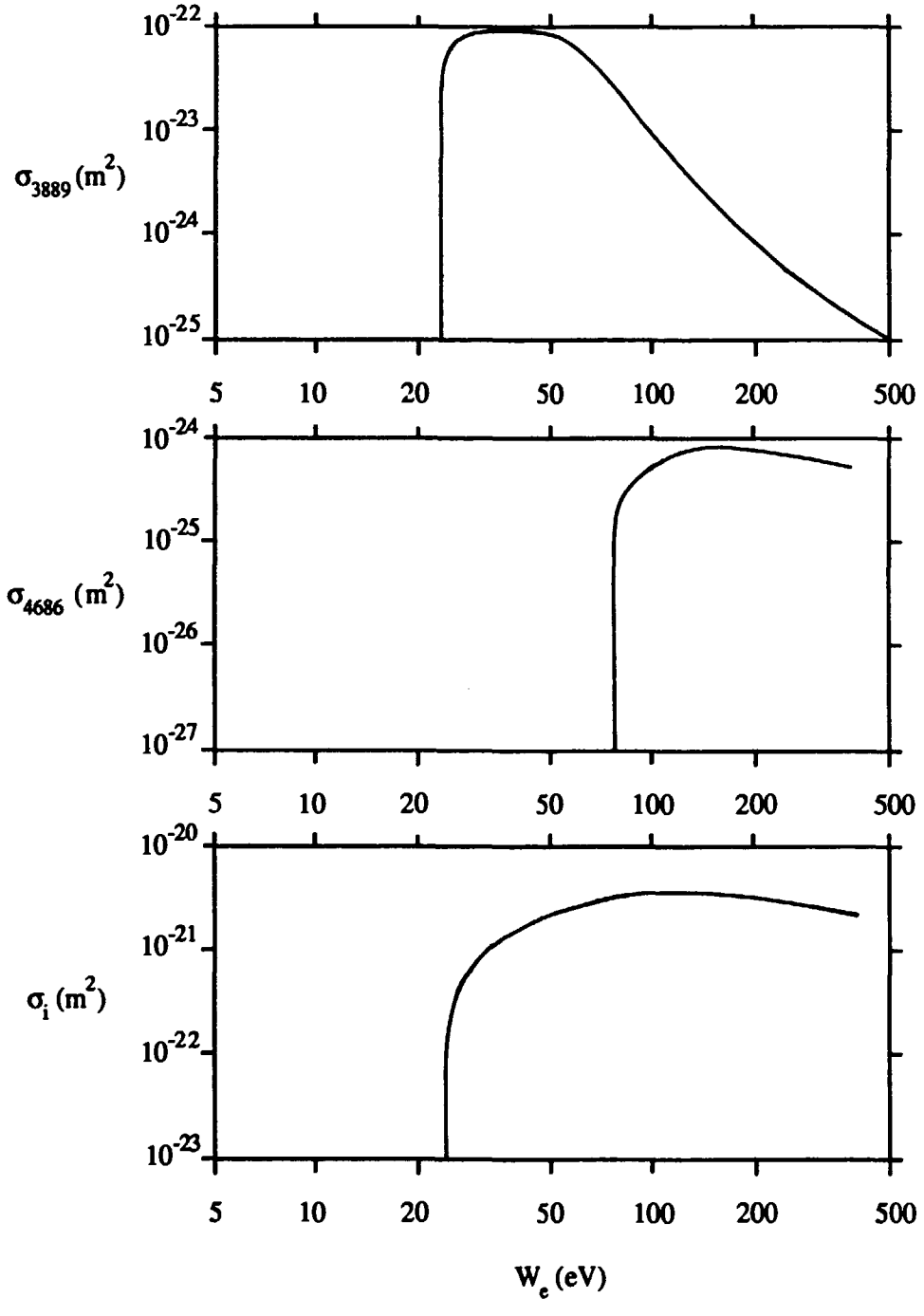

Fig. 5. Cross sections for electron impact excitation of the He I line 3889 Å, and the He II line 4686 Å, both from the ground state of He I, and for electron impact ionization.

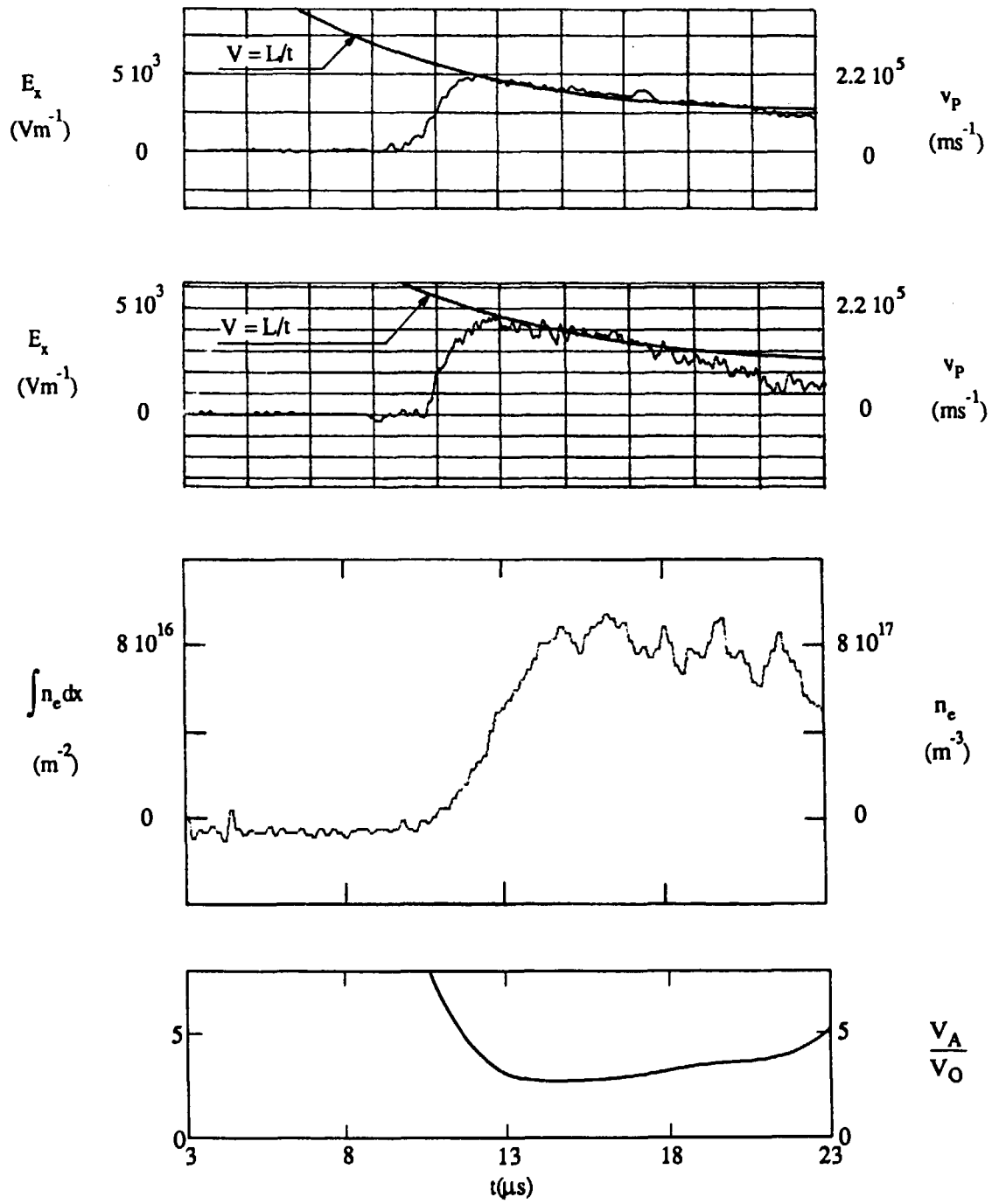

Fig. 6. Example of measurements of the undisturbed plasma stream

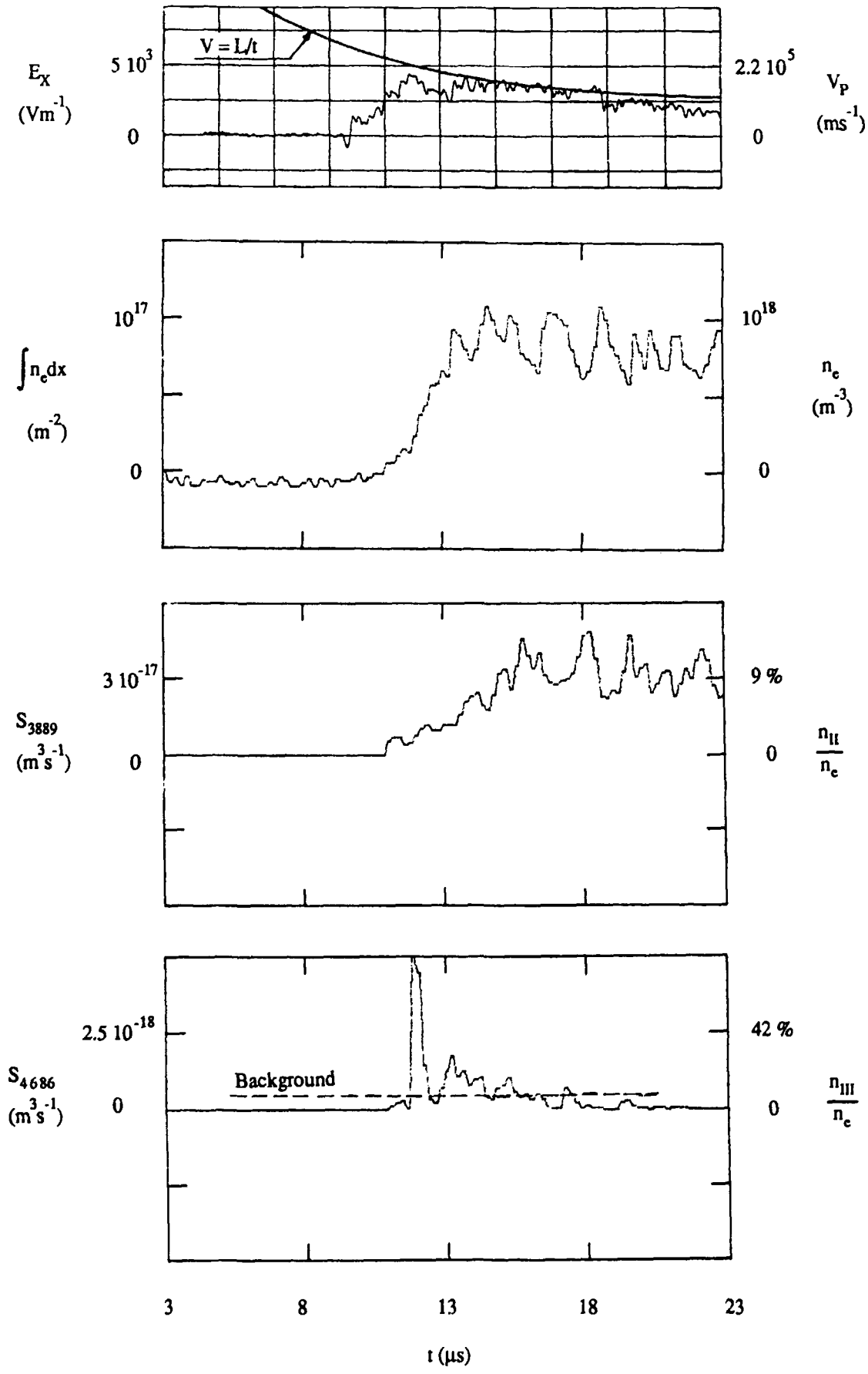

Fig. 7. Measurements for low column helium density. The scales to the left denote measured quantities, and the scales to the right calculated quantities. The relative populations n_{II}/n_e and n_{III}/n_e are derived from Eq. 4 and 5. For n_{II}/n_e, the scale is only accurate before 13 ms; for later times, the experimental curve is an upper limit to the real n_{II}/n_e.

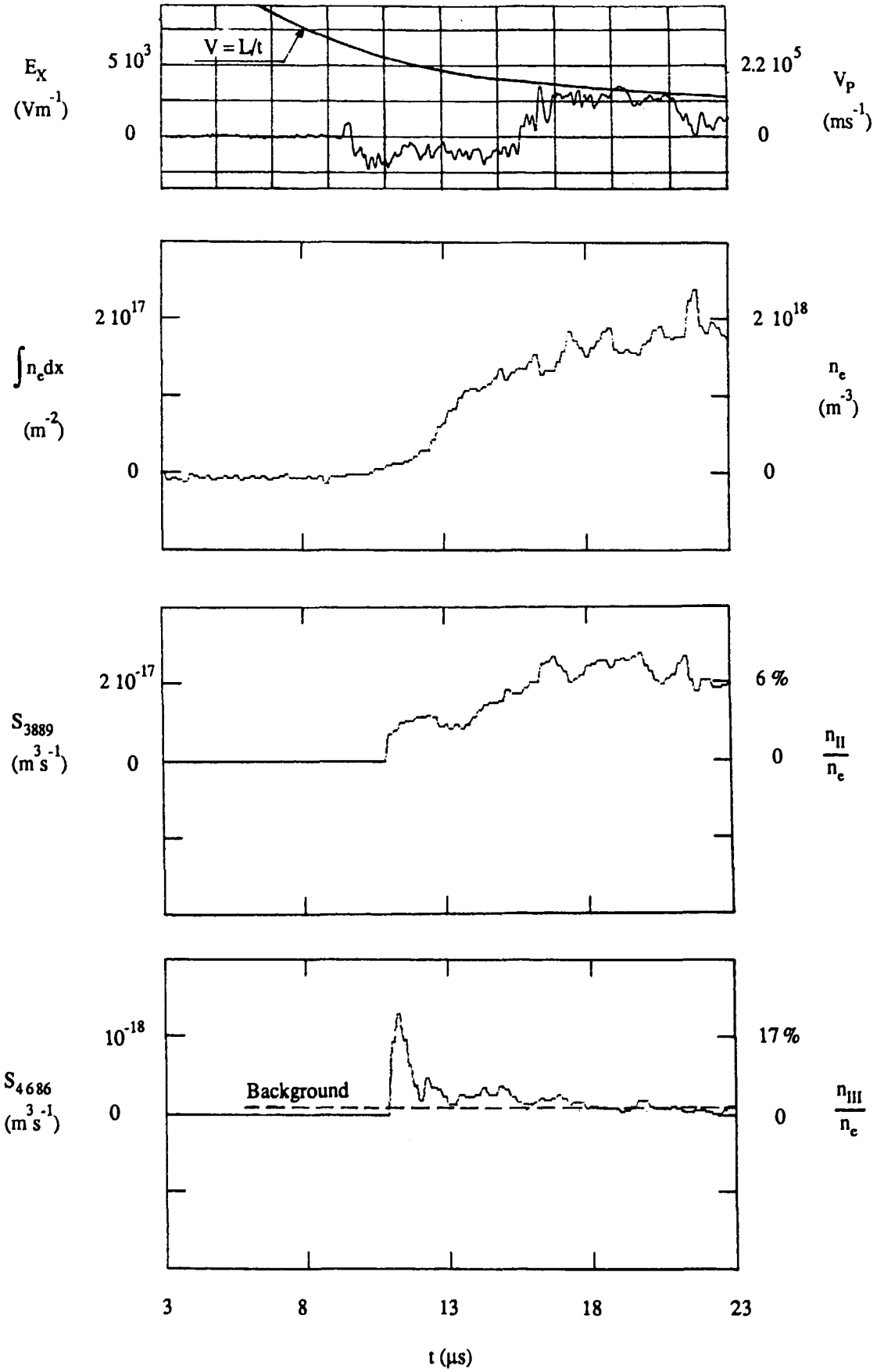

Fig. 8. Measurements for medium column helium density.

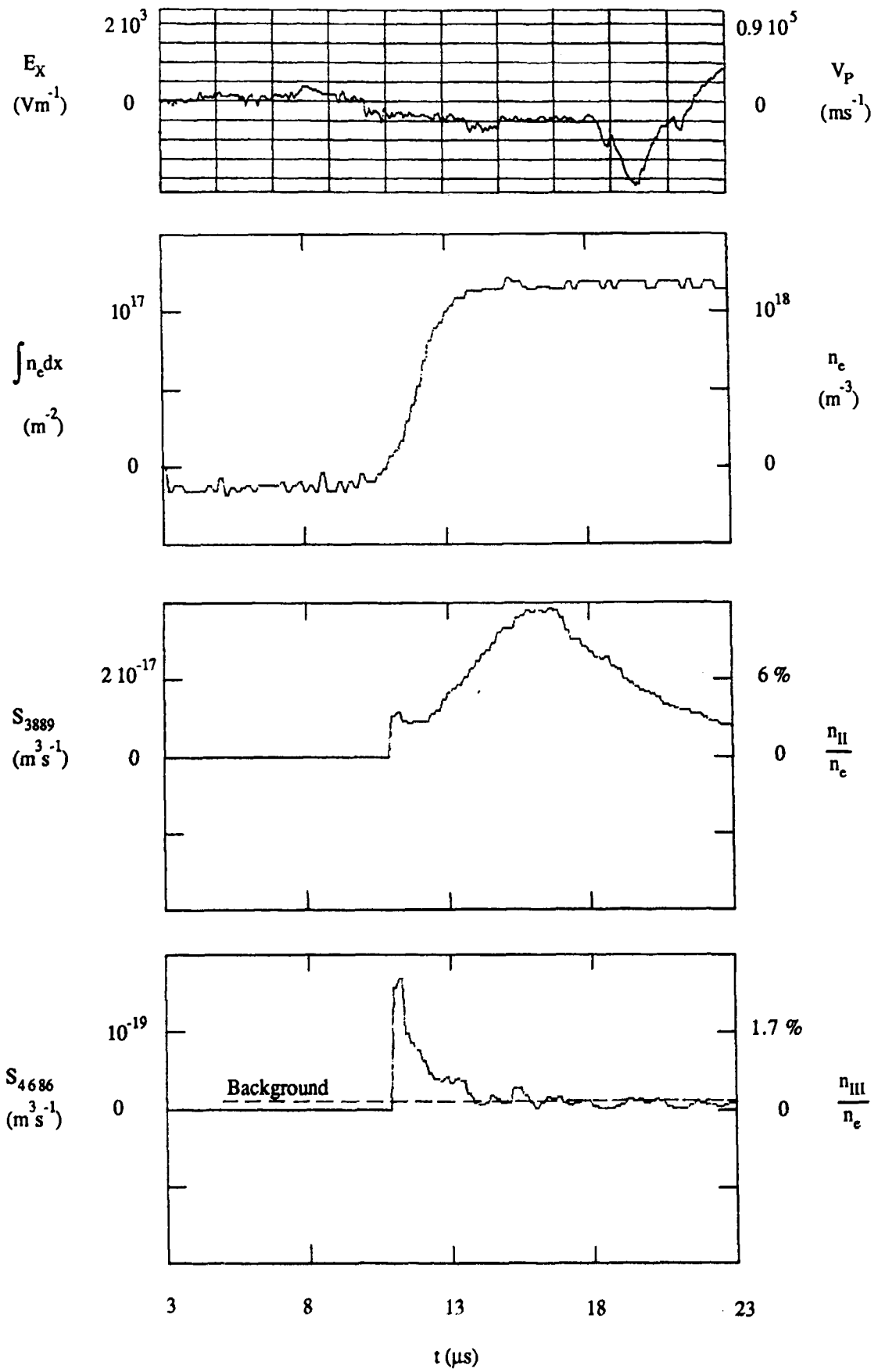

Fig. 9. Measurements for high column helium density.

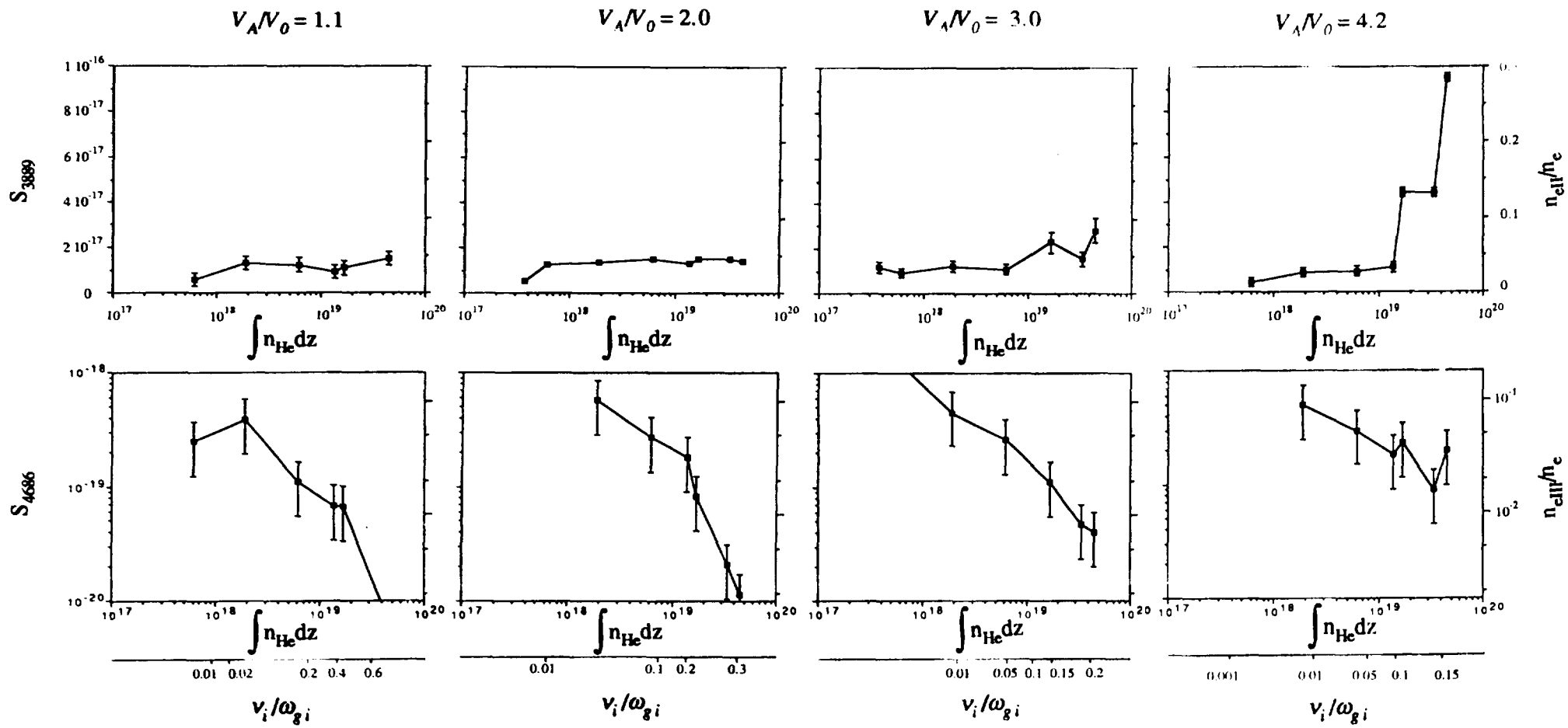

Fig. 10. Results from experiments with four different values of V_A/V_0.. The normalized ionization rates ν_i/ω_{gi} given at the bottom of the columns corresponds to the initial plasma stream. All figures in the same row have the same scales. The scales to the left are the effective excitation rates as defined in the text, and the scales to the right show the relative populations I (25 - 75 eV) and II (above 75 eV).

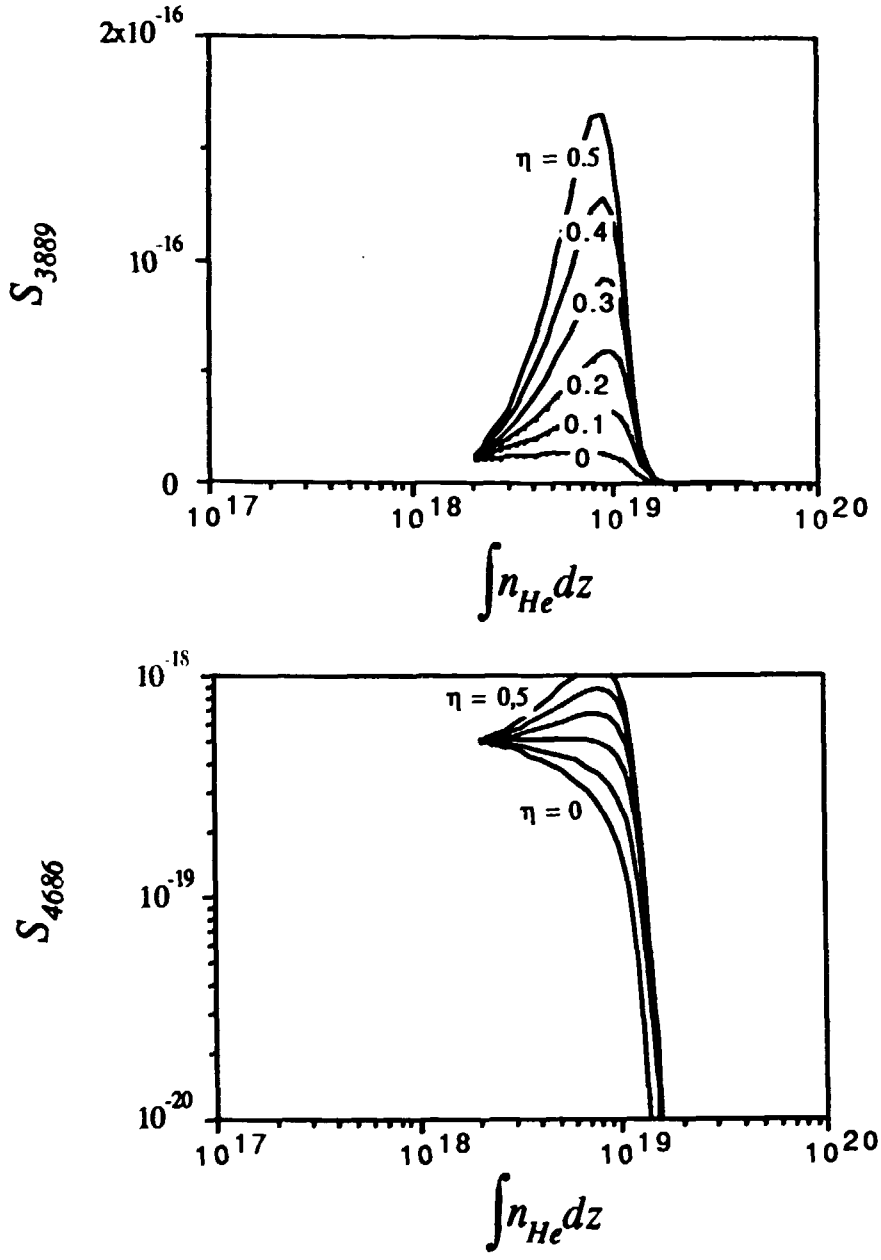

Fig. 11. Model calculations of the S_λ values as function of the neutral column density, using the initial values for the plasma stream of Fig. 10.

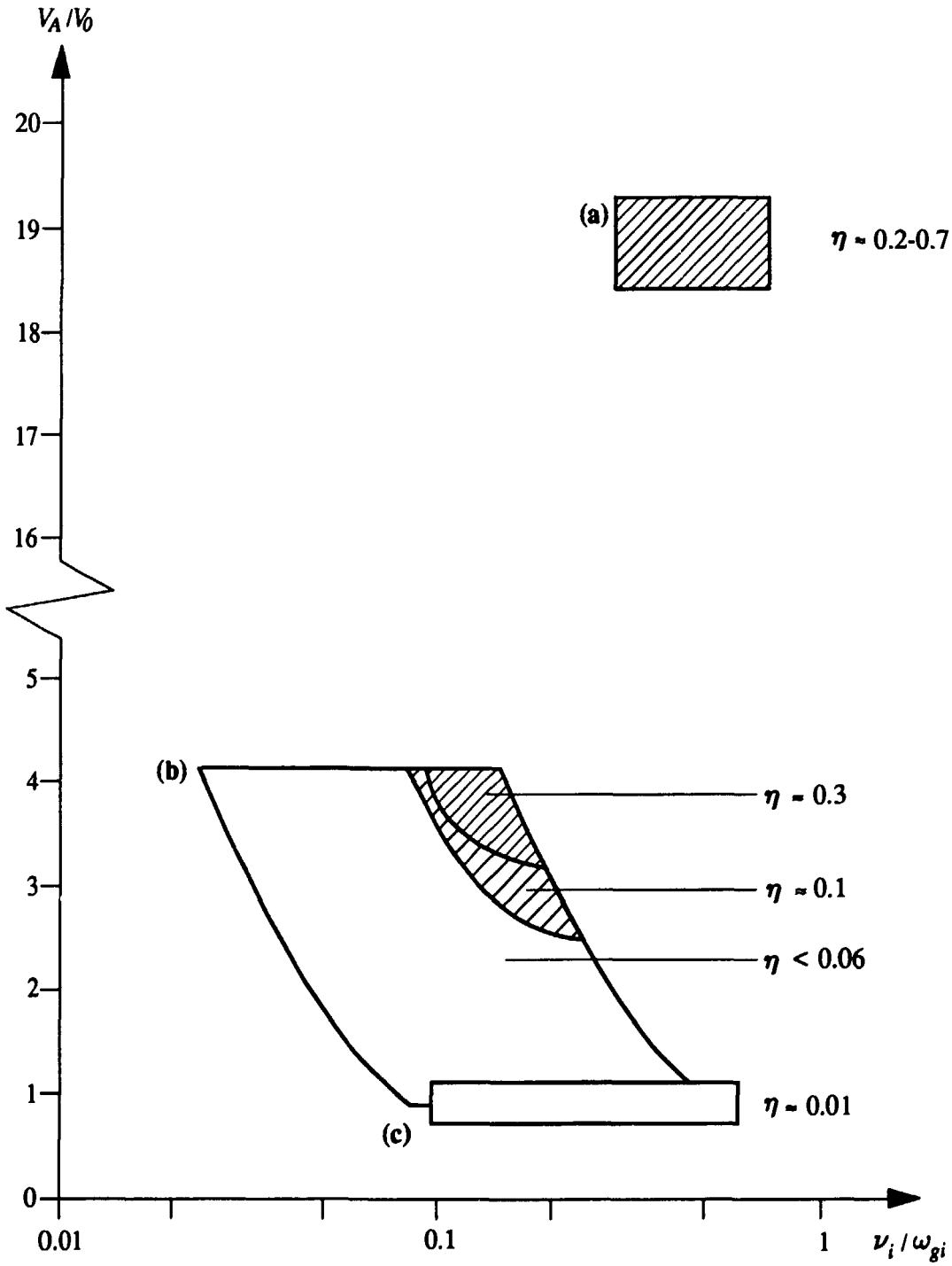

Fig. 12. The η value as function of V_A/V_0 and ν_i/ω_{gi}.(a): The experiments by Danielsson, 1972, and Danielsson and Brenning, 1975. (b): The present experiments. (c): The experiments by Brenning, 1981b.

TRITA-EPP-90-01 ISSN 0348-7539

The Royal Institute of Technology, Department of Plasma Physics,
S-100 44, Stockholm, Sweden.

LABORATORY EXPERIMENTS ON THE MAGNETIC FIELD AND NEUTRAL DENSITY LIMITS ON CIV INTERACTION

I. Axnäs and N. Brenning

March 1990, 40 pages incl. ill., in English.

Laboratory experiments are reported which determine the magnetic field and neutral density limits for Critical Ionization Velocity (CIV) interaction in the impact configuration. A combination of microwave interferometry and spectroscopy has been used to measure how the electron energy distribution varies with the neutral density and the magnetic field strength. The efficiency of the CIV process is evaluated in terms of the efficiency factor η of energy transfer to the electrons. This efficiency is studied as function of the ratio V_A/V_0 between the Alfvén velocity and the plasma stream velocity and the ratio ν_i/ω_{gi} between the ionization frequency and the ion gyro frequency. With other parameters kept constant, V_A/V_0 is proportional to the square root of the magnetic field, while ν_i/ω_{gi} is proportional to the neutral density. We have found that these two dimensionless parameters are coupled in such a fashion that a stronger magnetic field can compensate for a lower neutral density. For our strongest magnetic field, corresponding to $V_A/V_0 = 4$, CIV interaction is found to occur for a comparatively low value $\nu_i/\omega_{gi} \approx 0.1$. For $V_A/V_0 = 1$, we found a clear absence of CIV interaction even for ν_i/ω_{gi} approaching unity.

Key words: Critical Velocity, Critical Ionization Velocity, Alfvén's Critical Velocity, CIV, Plasma-Neutral Gas Interaction.